HILLSLOPE CHARACTERISTICS AND BEHAVIOR IN RELATION TO NONLOCAL SEDIMENT TRANSPORT

By

Tyler H. Doane

Thesis

Submitted to the Faculty of the

Graduate School of Vanderbilt University

in partial fulfillment of the requirements

for the degree of

MASTER OF SCIENCE

in

EARTH AND ENVIRONMENTAL SCIENCES

August, 2014

Nashville, Tennessee

Approved:

Dr. David Jon Furbish

Dr. Daniel Morgan

This thesis is dedicated to

all the unnammed hills.

Acknowledgements

I would first of all like to thank Dr. David Furbish for his persistent support and guidance throughout this project. In pursuing this particular problem, Dr. Furbish has given me a unique perspective that has profoundly impacted how I view the world. I can only hope that as I continue to conduct research that I do it with such grace and motivation! Many thanks to him!

Secondly, I must take a moment to thank my colleagues at Vanderbilt for the support and community that they provided. Discussions with all of my fellow students often helped to foster new ideas or encourage further explorations. In particular Siobhan Fathel and Angel Abbott aided in my project and developing ideas.

I would like to thank the faculty at Colorado College who provided the initial motivation for me to study Geology. They have had a profound impact on my life and continue to be a source of guidance. I look forward to continued discussions with them in the future and thank them for their unyielding support.

I also received a great amount of help and material from Simon Mudd and Stuart Grieve, and Josh Roering and Jill Marshall, who provided processed LiDAR datasets of the Coweeta Hydrologic Lab area and a portion of the Oregon Coast Range respectively.

Lastly, I owe a great deal to my family for providing an immense amount of support and encouraging me to pursue this path. It is a privilege to have a family that can see my passion and encourage me to follow it in challenging moments. I am fortunate to have had such great support throughout my pursuits.

Table of Contents

List of Figures

Part I

Hillslope Form and Relief

Chapter 1

INTRODUCTION

Formulations for the hillslope sediment flux are central in understanding the form and evolution of Earth's surface. Sediment transport processes continuously redistribute unconsolidated mass and thereby constantly transform the land surface. The form of a landscape in turn reflects the processes that shaped it. The connection between process and form is a cornerstone of geomorphology and motivates research that pursues a mathematical understanding of transport processes.

Following the suggestion of Culling [1965], researchers commonly describe the rate of hillslope sediment transport on soil-mantled hillslopes as a linear function of the local land-surface slope. This has led to the widespread use of a local, linear hillslope diffusion equation to describe hillslope sediment transport. For steady state conditions, diffusive sediment transport processes create parabolic hillslope profiles where the land-surface slope increases linearly with distance from the ridge. However, in steepland settings, hillslopes have distinctly non-parabolic profiles that become increasingly linear downslope. This simple observation is a source of dissatisfaction with a local, linear diffusive formulation for the hillslope sediment flux [*Roering et al.*, 1999; *Tucker and Bradley*, 2010; *Furbish and Haff*, 2010] and motivates research that pursues alternative descriptions.

Recent research suggests that there is value in using nonlocal formulations for the hillslope sediment flux [*Foufoula-Georgiou et al.*, 2010; *Furbish and Roering*, 2013; *Tucker and Bradley*, 2010]. Whereas local formulations of sediment transport are expressed as a function of purely local conditions [eg. *Heimsath et al.*, 1997; *Roering et al.*, 1999], a nonlocal formulation considers the flux as a function of all upslope contributing positions. The concept of

nonlocal sediment transport arises from the notion that particles may travel sufficiently far such that motions are not accurately described by local hillslope conditions. These motions are more appropriately described as a function of the conditions at their release point or by the integrated conditions over which they travel. Sediment particle travel distance increases on steeper hillslopes [*Gabet and Mendoza*, 2012] such that the motions become increasingly nonlocal. Therefore, in steepland settings, a nonlocal formulation may more accurately describe sediment motions and consequently the hillslope sediment flux. Landscape evolution models that use a nonlocal formulation for the hillslope sediment flux produce hillslope profiles that are similar to steepland hillslopes observed in nature [*Furbish and Haff*, 2010], which warrants further exploration of nonlocal sediment transport.

Theory for nonlocal hillslope sediment transport has outpaced field or empirical studies designed to inform it. In this contribution, I pursue a better understanding of some of the key ingredients of a nonlocal formulation by investigating the form of many hillslopes in diverse settings. In particular, I show how central parameters in transport processes may be extracted from topographic data. Analogous to the method used by researchers to extract a hillslope diffusivity from hilltop curvature [*Roering et al.*, 2007], I extract a similar quantity that expresses the activity of transport mechanisms. This quantity is process-specific and therefore offers a connection between specific hillslope processes and fundamental hillslope characteristics such as relief and mean hillslope gradient.

Part I of this thesis is aimed at exploring particular quantities of different landscapes that will inform a nonlocal transport formulation. In chapter two, I highlight the major differences between local and nonlocal sediment transport. Although this topic is treated in previous research, it is useful to explain nonlocal transport with an understanding of local transport. In chapter three, I review the development of a nonlocal formulation. The formulation used in

this paper is presented in Furbish and Roering [2013], and closely follows their development. It is conceptually simple to develop a nonlocal formulation in the form of a convolution integral. However, it is analytically useful to recast the formulation into an advection-diffusion form to illustrate key behaviors and characteristics of nonlocal transport. For example, Furbish and Haff [2010] use the advection-diffusion form of a nonlocal formulation to derive an analytical solution for the steady-state topographic configuration of hillslopes and is described in chapter four. Chapter five tests their hypothesis that hillslope profiles exhibit an $x^{3/2}$ relationship with position x by extracting topographic profiles from diverse tectonic and climatic environments. In this section I also show how topographic profiles can provide important information about active transport processes, which provides strong links to hillslope relief.

In Part II, I explore the stability behavior of hillslopes that evolve largely by nonlocal sediment transport. That is, I investigate the response of hillslopes to perturbations about a steady-state configuration. An unstable process amplifies perturbations with time whereas a stable process tends to attenuate the perturbations and the land-surface returns to the initial state. Local, linear diffusion is unconditionally stable [*Furbish and Fagherazzi*, 2001], but the behavior introduced by nonlocal sediment transport formulations remains unknown. Any instability introduced by the transport mechanism is expected to be reflected in the spatial distribution of soil thickness in addition to the land-surface configuration. The spatial distribution of soil thickness is often used to evaluate the evolutionary state of a landscape (steady versus transient) [*Heimsath et al.*, 2001]. However, if nonlocal sediment transport introduces some instability to the land-surface, the soil thickness may be spatially variable, but does not necessarily preclude a landscape from being in an approximate steady state.

Chapter 2

LOCAL VERSUS NONLOCAL TRANSPORT

It is important to first make a distinction between local and nonlocal transport. A physical distinction between the two concepts is difficult to definitively draw and is addressed in previously published literature [*Furbish and Roering*, 2013]. A mathematical distinction is simpler to define and is reviewed here.

Culling [1965] reasoned that particles within a soil column experience quasi-random motions due to the creation and collapse of pore space. The average particle displacement for these motions is on the order of the average pore diameter. Inasmuch as the pore diameters within soil columns are far smaller than the average thickness of the soil mantle, we may describe the rate of soil creep as a *local* expression. That is, the rate of sediment transport at x, a horizontal position, is accurately described as a function of hillslope conditions at x only. The vertical structure of soil columns yields a systematic increase of particle concentration with depth, the contours of which are parallel to the land-surface slope. Active lofting motions on average loft particles in a direction normal to the concentration gradient. Settling motions are, for the most part, passive and vertically downward which ultimately results in a bulk downhill motion [*Furbish et al.*, 2009a] (Figure 1). This leads to a slope-dependent transport formulation in the form of the familiar linear diffusion equation [*Culling*, 1965]

$$q_x = -D\frac{\mathrm{d}\zeta}{\mathrm{d}x}, \tag{2.1}$$

where q_x [$\mathrm{L}^2\ \mathrm{T}^{-1}$] is the hillslope sediment flux, ζ [L] is the land-surface elevation, x [L] is a coordinate position that is downslope, and D is like a diffusivity [$\mathrm{L}^2\ \mathrm{T}^{-1}$]. Local diffusive

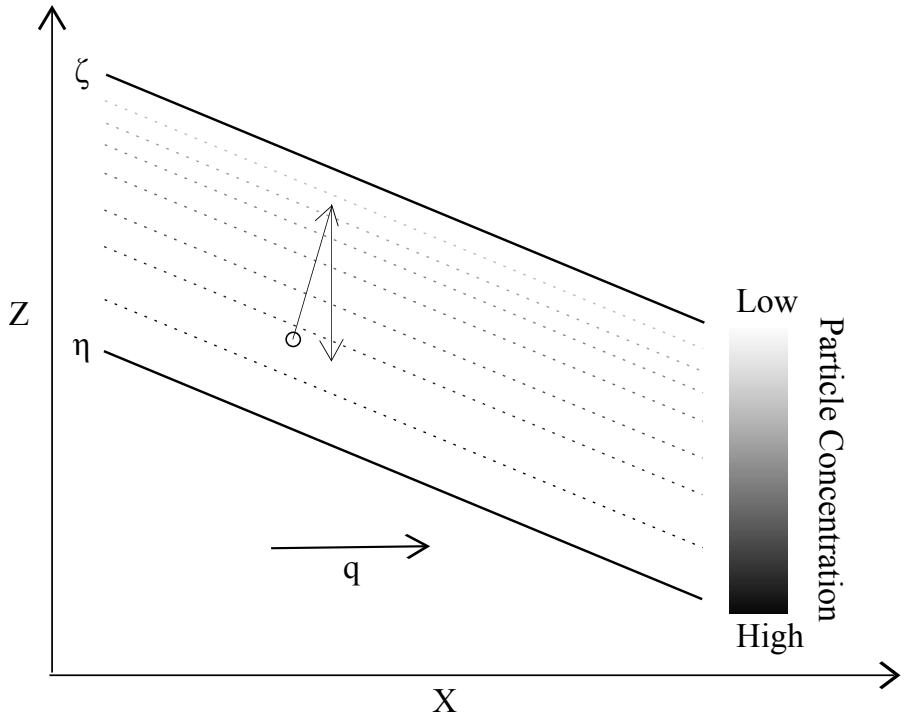

Figure 1: Diagram explaining how slope dependent transport arises from quasi-random particle motion. ζ is the land-surface, η is the soil-saprolite surface, Z and X are vertical and horizontal coordinate axes.

descriptions of the rate of sediment transport have a strong legacy and are common in geomorphology. Similarly, sediment transport due to rain splash leads to a slope dependent transport formula similar to (2.1) [*Furbish et al.*, 2009b].

There are, however, sediment particle motions that (2.1) does not account for. In steepland and post-fire settings, particles displaced on the surface may travel distances many times the average pore diameter in the soil column (e.g. motion due to dry ravel, tree throw, overland flow, soil slips). In this case, particles that contribute to the flux at position x began their motions at some upslope position x' which may possess different hillslope conditions. Thus an attempt to describe particle motions as a function of local conditions at position x does not accurately account for the motions of those particles that travel significant distances. In certain settings, nonlocal sediment particle motions may dominate the flux, which warrants the development of a formulation that describes nonlocal sediment particle motions.

Researchers have indirectly attempted to address nonlocal sediment particle motions with the development of local nonlinear slope-dependent transport models [*Roering et al.*, 1999]. These models are motivated by the observation that hillslopes become increasingly linear as slopes approach a critical magnitude, S_c. Surfaces that approach S_c generate high transport rates which do not allow the land-surface to further steepen and therefore create an increasingly linear hillslope profile. Although it is not explicit in these models, these models call on increasing particle travel distances that result from processes such as small landslides [*Roering et al.*, 2001]. A one-dimensional nonlinear formulation for the hillslope flux is expressed as [e.g. Roering et al., 1999],

$$q_x = \frac{D\frac{\mathrm{d}\zeta}{\mathrm{d}x}(x)}{1-\left(\frac{|\frac{\mathrm{d}\zeta}{\mathrm{d}x}(x)|}{S_c}\right)^2}. \tag{2.2}$$

Equation 2.2 is a local formulation, as the flux at x is solely a function of hillslope conditions at x. The motions it invokes are nonlocal yet the formulation does not include any description of particle motions. Whereas this class of nonlinear models effectively introduces the notion of increasing particle travel distance with increasing slope, it lacks the physical basis that describes particle motions and is therefore not mass-conserving.

Consider a convex-concave soil-mantled hillslope (Figure 2). Let us pick two positions x_1 and x_2 that possess the same conditions, namely the same local land-surface slope. Although their local slopes are identical, the upslope topographic configuration differs between these two points. Now consider a number of particles released from position $x_1' = x_1 - r$, where r is a travel distance. Each particle that is now in motion has a distinct probability of travelling at least a distance of r, in which case it would contribute to the flux at x_1. Let us release the same number of particles from position $x_2' = x_2 - r$, which is equally far upslope. Because conditions at x_2' differ from those at x_1', the probability of particles travelling at least a distance of r is

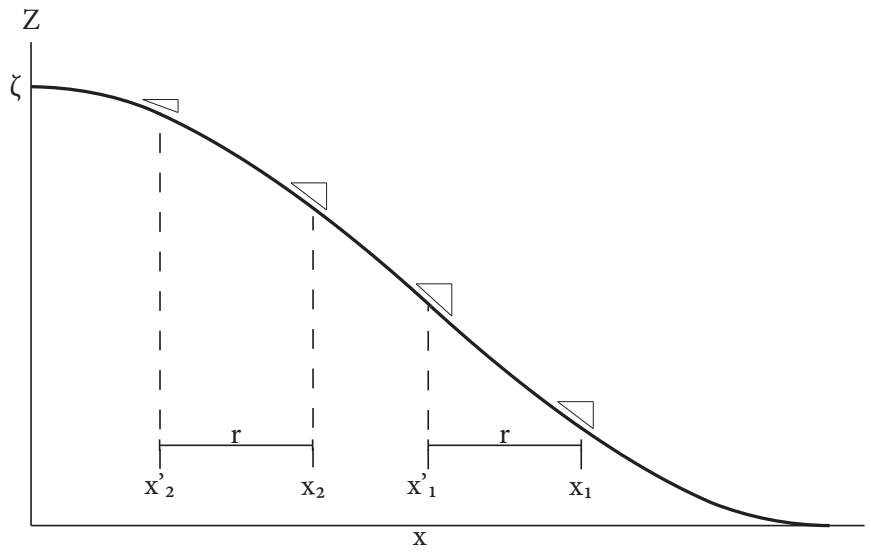

Figure 2: Diagram showing the land-surface profile with positions x_1 and x_2 exhibiting the same local slopes but different up slope configurations.

different from those released from x_1', and therefore x_1 and x_2 receive different amounts of sediment from positions a distance r upslope. If we vary r such that $x - r = x'$ refers to every point along the hillslope, we will likely see that x_1 and x_2 rarely receive the same contribution of sediment from upslope, and therefore the flux at x_1 and x_2 are likely to differ. Thus the flux is not only a function of conditions at x_1 and x_2, but must include the weighted conditions of all positions on the hillslope. Two key ingredients, a sediment particle entrainment rate and a probability density function (pdf) of particle travel distances, can be used to probabilistically account for all entrained particles. In doing so, a nonlocal formulation provides a physically-based description the flux that includes nonlocal travel distances. Mathematically this may be expressed as a convolution integral

$$q(x,t) = \int_{-\infty}^{x} h_r(x - x')E[S(x), x']\mathrm{d}x', \tag{2.3}$$

where E is a sediment particle entrainment rate [$\mathrm{L}^3\ \mathrm{L}^{-2}\ \mathrm{T}^{-1} = \mathrm{L}\ \mathrm{T}^{-1}$], x' denotes some

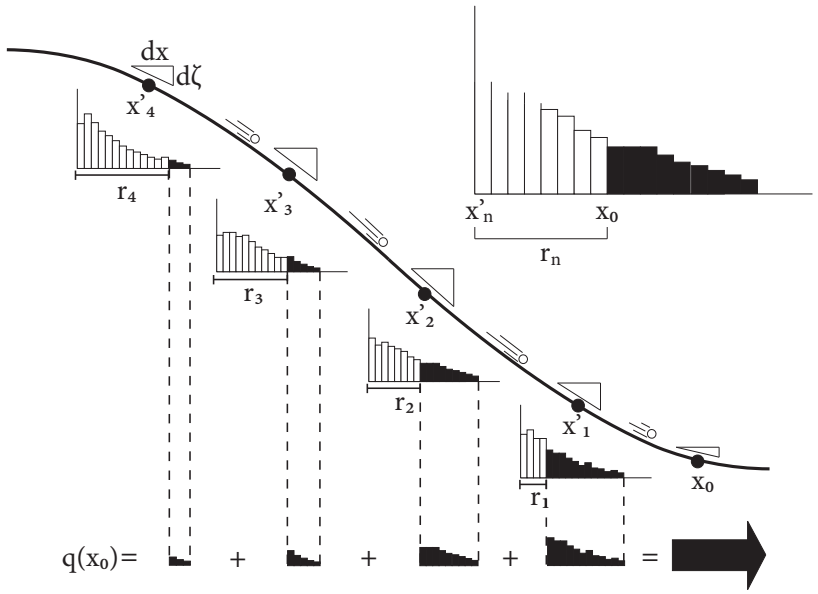

Figure 3: Diagram showing the land-surface configuration and contributions to the flux at position x_0 from all upslope positions. Portions of the pdf's of particle travel distance from each release point contribute to the flux at x_0.

position upslope of x, $S = \mathrm{d}\zeta/\mathrm{d}x$ is the land-surface slope and h_r is a kernel that properly weights the contributions to the flux at x (Figure 3). By integrating the convolution over all upslope positions, (2.3) includes the motions of particles released from all positions that contribute to the flux at position x. Although not a statement of conservation of mass, (2.3) is mass conserving. The following section highlights the components and development of a nonlocal formulation, which requires physically-minded expressions for the entrainment rate and a disentrainment rate.

Chapter 3

DERIVING A NONLOCAL FORMULATION

The Survival Function

A nonlocal formulation of sediment transport attempts to describe the motion of every sediment particle entrained during a specified time interval. However, understanding the physics of individual sediment particle motions over geomorphic time scales is unrealistic. We can, however, take a probabilistic approach that reflects the characteristic behavior of particles over long timescales. The foundations of the probabilistic approach are based on a kinematic description of sediment motions. To probabilistically describe motions, I rely on a probability density function (pdf) that describes the likely travel distance of sediment particles. The pdf represents a sample of travel distances taken over a sufficiently long time such that the form of the pdf becomes invariant with time. That is, the pdf is a smooth function that represents a large number of particle motions such that subsequent motions do not appreciably change the mean or variance. We begin with a physical description of the sediment particle disentrainment rate [*Furbish and Roering*, 2013]. Noting that a disentrainment rate, P_r, may be interpreted as a failure rate, it is defined as

$$P_r(r;x') = \frac{f_r(r;x')}{1-F_r(r;x')} = \frac{f_r(r;x')}{R_r(r;x')}, \tag{3.1}$$

where f_r is a pdf of travel distances r, F_r is the cumulative distribution function of r, and R_r is the survival function. P_r describes the likelihood that a particle in motion will come to rest within $r + \mathrm{d}r$, given that it has travelled, or 'survived', a distance r already. This defines a conditional probability represented by the right-most portion of (3.1). The probability

distrubution function $f_r(r;x') = dF_r(r;x')/dr = -dR_r(r;x')/dr$ so that

$$P_r(r;x') = -\frac{1}{R_r(r;x')}\frac{dR_r(r;x')}{\mathrm{d}r}. \tag{3.2}$$

The pdf of particle travel distances may be retrieved from (3.2) by integrating once, namely,

$$f_r(r;x') = P_r(r;x')e^{-\int_0^r P_r(w;x')\mathrm{d}w}. \tag{3.3}$$

Furthermore, the survival function is related to (3.3) by $R_r(r;x') = f_r(r;x')/P_r(r;x')$. This allows us to define a survival function directly from a disentrainment rate,

$$R_r(r;x') = e^{-\int_0^r P_r(w;x')\mathrm{d}w}. \tag{3.4}$$

Therefore, we can develop a probabilistic description of particle travel distances from a spatial particle disentrainment rate. The disentrainment rate is a function of position for reasons presented in the next section.

The Disentrainment Rate

The development of a disentrainment rate is key for the development of a sound nonlocal formulation for the hillslope sediment flux. The disentrainment rate used here and developed in Furbish and Haff [2010] is based on the notion that sediment particles in motion tend to travel farther on steeper surfaces [*Gabet and Mendoza*, 2012]. That is, the probability of disentrainment is lower on steep slopes. Consequently, slope has a first order influence on disentrainment rate, which may be expressed as [*Furbish and Roering*, 2013]

$$P_r(r;x') = \frac{1}{\lambda_0}\left(\frac{2S_c}{S_c - S(x')} - 1\right), \tag{3.5}$$

where λ_0 is the average particle travel distance on a horizontal surface for a given process, and S_c is the magnitude of a critical slope above which particles continue to travel indefinitely. The critical slope coincides with S_c from *Roering et al.*, 1999. Equation 3.5 is a parsimonious description of disentrainment. It does not explicitly treat any effect that factors such as the particle size distribution, surface roughness, or soil type may have on the behavior of moving particles. However, to avoid the risk of being unnecessarily heuristic, I argue that (3.5) is a judicious description of the particle disentrainment rate.

Inserting (3.5) into (3.4) retrieves a survival function of sediment particle travel distances for those released from x', namely,

$$R_r(r;x') = e^{-\frac{1}{\lambda_0}\int_0^r \left(\frac{2S_c}{S_c - S(x')} - 1\right) \mathrm{d}w}. \tag{3.6}$$

Making use of (3.3), we can obtain the pdf of particle travel distances,

$$f_r(r;x') = \frac{1}{\lambda_0}\left(\frac{2S_c}{S_c - S(x')} - 1\right) e^{-\frac{1}{\lambda_0}\left(\frac{2S_c}{S_c - S(x')} - 1\right)\int_0^r \mathrm{d}w}. \tag{3.7}$$

The form of the pdf is exponential, but as the magnitude of S increases, probability is shifted towards the tail. For all slopes below S_c, the distribution has a defined mean and variance, which, by definition, remains exponential and is not heavy-tailed. This is in contrast with previous nonlocal formulations [*Foufoula-Georgiou et al.*, 2010; *Tucker and Bradley*, 2010] which define nonlocal transport as necessarily involving a heavy-tailed pdf of particle travel distances. Nonetheless, the mean particle travel distance and variance become undefined when $|S| \to S_c$, which is consistent with the concept that particles remain entrained indefinitely [*Roering et al.*, 2001].

Entrainment Rate

Particles are set in motion by some disturbance. Such disturbances in hillslopes are stochastic in space and time, but over sufficiently long timescales we assume that the number of disturbances per unit area approaches a steady value. The entrainment rate, E [$\mathrm{L}^3\mathrm{L}^{-2}\mathrm{T}^{-1}$], reflects the frequency of such disturbances. It is composed of two parts; a background entrainment rate E_0 and a slope-dependent entrainment rate E_1. On a flat surface, the background entrainment rate E_0 accounts for all entrained particles. Where the land-surface is sloped, the slope-dependent term adds to the background rate as a linear function of slope. The total entrainment rate, E, is expressed as,

$$E(x') = E_0 + E_1|S(x')| \tag{3.8}$$

Writing the entrainment rate as a linear function of slope reflects the notion that as slopes steepen, the tangential force required to move a particle is reduced, and therefore more particle entraining disturbances are likely to occur. Other functional forms of entrainment rate may be appropriate, but (3.8) is a simple and physically-based form. It is important to note that an entrained particle does not necessarily need to be displaced. That is, it may have a travel distance of zero.

The complete convolution integral is formed by integrating the product of (3.4) and (3.8) over space,

$$q_x(x) = \int_{-\infty}^{x} \left(E_0 - E_1 S(x')\right) e^{-\frac{x-x'}{\lambda_0}\left(\frac{S_c}{S_c - S(x')} - 1\right)} \mathrm{d}x' \qquad S(x') \leq 0. \tag{3.9}$$

Integrating from $-\infty$ to x accounts for the contributions of sediment released from all positions

upslope of x to the flux at position x.

Chapter 4

STEADY STATE CONFIGURATION

Although this convolution integral for the hillslope sediment flux is a comprehensive description of motions, it is somewhat cumbersome to work with as it requires numerical integration and hinders simple analytical solutions. In many cases, an approximation of (3.9) is sufficient to highlight the essential behaviors and characteristics of hillslopes that evolve by nonlocal particle motions. Furbish and Haff [2010] show that a Taylor expansion of (3.9) recasts the formulation into the more common Fokker-Planck (or advection-diffusion) form. Furbish and Roering [2013] formally demonstrate that this operation retrieves the mean and raw variance of particle travel distance as components of the advective and diffusive terms respectively. The flux is approximated by

$$q_x(x) = E(x)\mu_r(x) - \frac{1}{2}\frac{\mathrm{d}}{\mathrm{d}x}\left[E(x)\sigma_r^2(x)\right], \tag{4.1}$$

where μ_r and σ_r^2 are the first and second moments of particle travel distance. Taking into account positive and negative motions, the mean travel distance is

$$\mu_r(x) = -\lambda_0 S(x)\left(\frac{2}{S_c} + \frac{1}{kS_p}\right), \tag{4.2}$$

where S_p is a slope magnitude above which all particle motion is downslope, and k is a modulating factor. The raw variance goes as,

$$\sigma_r^2 = 1 + \frac{4S(x)^2}{S_c^2} + \frac{4S(x)^2}{kS_pS_c}. \tag{4.3}$$

A complete derivation of (4.2) is presented in Furbish and Roering [2013]. Substituting (4.2) and (4.3) into (4.1) gives

$$\begin{aligned} q_x(x) &= (E_0 - E_1 S(x)) \left[-\lambda_0 S(x) \left(\frac{2}{S_c} + \frac{1}{kS_p} \right) \right] \\ &- \frac{1}{2} \frac{d}{dx} \left[(E_0 - E_1 S(x)) \left(1 + \frac{4S(x)^2}{S_c^2} + \frac{4S(x)^2}{kS_p S_c} \right) \right] \qquad S \leq 0. \end{aligned} \tag{4.4}$$

Furbish and Haff [2010] show that the advective part of (4.4) dominates the flux such that the diffusive part becomes negligible.

Hillslopes in steady-state satisfy the condition $q_x(x) = c_\eta W x$, where c_η is the particle concentration at the soil-saprolite boundary and W is the uplift rate. The steady-state configuration of slope can be solved by using (4.4),

$$c_\eta W x = (E_0 - E_1 S(x)) \left[-\lambda_0 S(x) \left(\frac{2}{S_c} + \frac{1}{kS_p} \right) \right]. \tag{4.5}$$

Further assuming that $E_1 \gg E_0$, then (4.5) becomes,

$$c_\eta W x = -E_1 S^2(x) \lambda_0 \left(\frac{2}{S_c} + \frac{1}{kS_p} \right). \tag{4.6}$$

Isolating S and integrating with respect to x once retrieves the land-surface elevation,

$$\left[\frac{c_\eta W}{E_1 \lambda_0 \left(\frac{2}{S_c} + \frac{1}{kS_p} \right)} \right]^{\frac{1}{2}} \frac{2}{3} x^{\frac{3}{2}} = Z_0 - \zeta(x). \tag{4.7}$$

The term on the left hand side of (4.7) is referred to as the drop-from-ridge, Z_d (i.e. the relief from the ridge top to x) and has the relation $Z_0 - Z_d(x) = \zeta(x)$ where Z_0 is the ridge-top

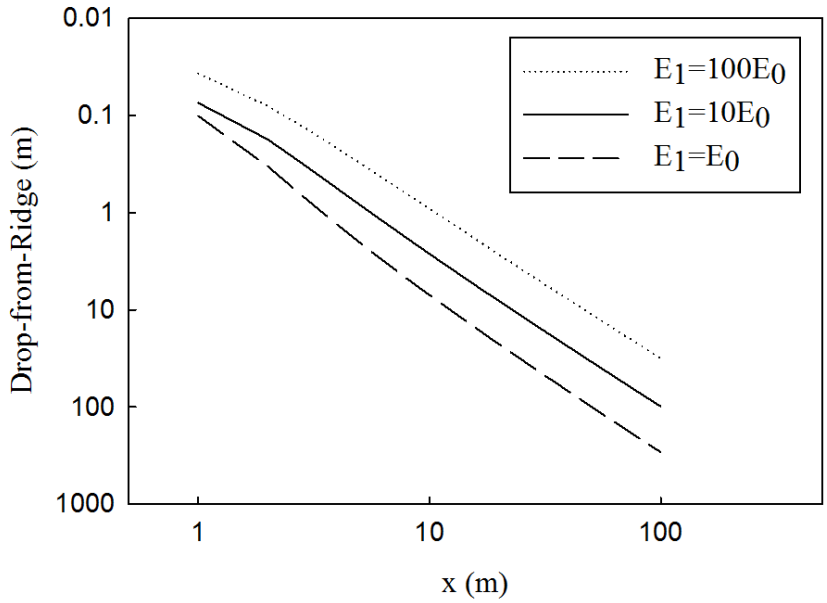

Figure 4: Drop-from-ridge versus position in log-log space reveals best-fit logarithmic relationships that are distinctly non-parabolic. For $E_1 = 100E_0$, 1.53; for $E_1 = 10E_0$, 1.59; for $E_1 = E_0$, 1.68

elevation.

The exponent on x in (4.7) determines the form of the hillslope, that is, the geometrical configuration. For a linear diffusive formulation, Z_d has an x^2 relationship, which gives a parabolic form of hillslopes. The convenient analytic approximation of the steady state configuration, (4.7), highlights a fundamental difference between local and nonlocal formulations; that hillslopes display non-parabolic forms with an $x^{3/2}$ relationship.

Whereas (4.7) is successful in highlighting an essential behavior of hillslopes, it neglects E_0 and the second order term of (4.4), which is an approximation itself. Including these terms requires a numerical solution for the steady state configuration that does not obey a simple power relationship. As E_0 approaches E_1, the steady state configuration deviates from the analytical $x^{3/2}$ relationship. However, so long as $E_1 \gtrapprox E_0$, hillslopes remain distinctly non-parabolic (Figure 4).

In steepland settings, surface motions may comprise the time-averaged majority of bulk

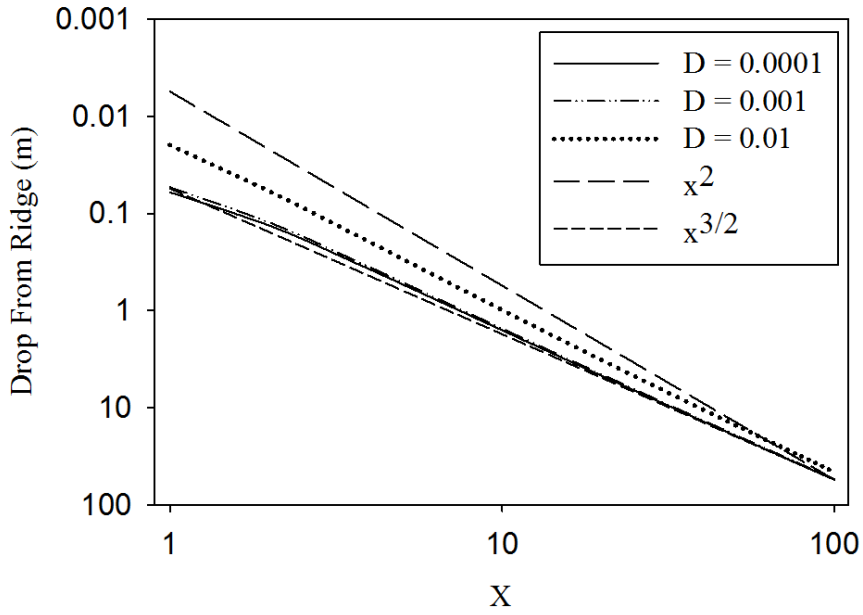

Figure 5: Drop-from-Ridge versus position in log-log space with varying diffusivities (D) for linear diffusive transport. Other parameteric values are $E_1 = 0.01$, $E_0 = 0.0001$, $W = 0.0001$, $\lambda_0 = 1$, $S_p = 0.4$, $S_c = 1.2$, and $k = 0.5$.

motions. However, local motions within the soil column still contribute to the flux and ought to be included in the calculation of the bulk flux. We can include these motions by adding a linear diffusive term, q_d, to (4.1), to more completely represent the time-averaged bulk flux, $q_b = q_i + q_d$ [*Furbish and Haff*, 2010]. Including this term also requires a numerical solution for the steady state configuration which is more complex than the simple power relationship suggested by (4.7). In log-log space, the theoretical $x^{3/2}$ and x^2 relationships plot as straight lines with slopes of 3/2 and 2 respectively. Adding a diffusive term to (4.7) results in hillslope profiles that deviate from a simple power relationship (Figure 5). The magnitude of the deviation is a function of the relative contributions of nonlocal and diffusive motions to the overall flux. This is effectively expressed as a Péclet Number formed by

$$Pe = \frac{E_1 \lambda_0}{D}, \tag{4.8}$$

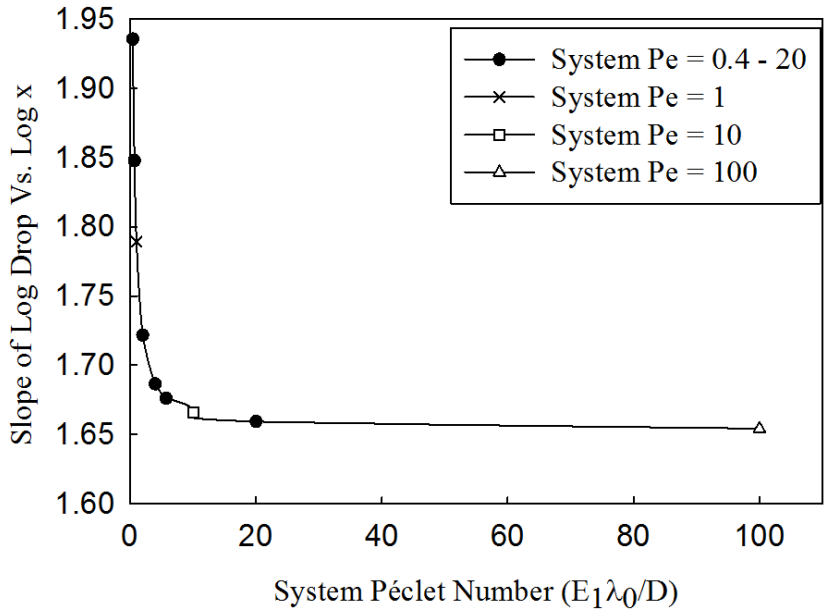

Figure 6: Plot of best-fit power relationships for drop-from-ridge versus position. The relationship becomes insensitive to variations in D when the Pe is greater than 10.

where the surface motions are analogous to advection. We imagine that D and $E_1\lambda_0$ are uniform throughout a landscape so that (4.8) is a system Péclet number (Pe).

Although combining linear diffusive and nonlocal transport draws steady state topography away from a simple power relationship, the deviations are quite small for most combinations of D and $E_1\lambda_0$. Thus, we can obtain a best-fit power relationship for drop-from-ridge and position that reflects the system Pe. For example, the stronger the nonlocal component the closer the best-fit power relationship is to $x^{3/2}$. Hillslope form is sensitive to Pe below 10. For Pe greater than 10, the best-fit power relationship asymptotically approaches a steady value that is around 1.5. Thus, for hillslopes with a form that is well described by a power law relationship close to the asymptotic value, we can say that Pe is large and that nonlocal motions dominate the bulk hillslope sediment flux (Figure 6).

Whereas the exponent on x in (4.7) determines the hillslope form, the parenthetical portion

determines the magnitude of the drop-from-ridge. As noted earlier, E_1 and λ_0 are specific to particular transport processes and their product gives the activity of the process. The parenthetical portion of (4.7) then is the ratio of uplift rate to transport activity, a quantity here termed R'. As this ratio increases, landscapes are expected to become characterized by increasingly greater hillslope relief and slopes. This is consistent with previous research which suggests that relief and slope, both hillslope and fluvial, is broadly determined by the competition between uplift and sediment transport [*Whipple et al.*, 1999; *Gabet et al.*, 2004; *Roering et al.*, 2007; *Ouimet et al.*, 2009]. Much of the physics of sediment transport in these studies is incorporated in dimensional coefficients that represent a rock erodibility (k) or a hillslope diffusivity (D). These terms, while convenient and capable of highlighting key behaviors and concepts, are a blackbox. A nonlocal formulation deconstructs the notion of a hillslope diffusivity into distinct components with physical interpretations which hold consistent dimensions. These components offer an opportunity to draw explicit connections between transport behavior and hillslope relief and slope.

Chapter 5

HILLSLOPE PROFILES

Here I present data from a large number of contour-normal topographic profiles taken from planar hillslopes. This dataset effectively tests the hypothesis that hillslopes in steepland settings have a form that is consistent with the non-parabolic form presented in the previous chapter. Theory suggests that, so long as nonlocal motions dominate the flux, hillslope form is insensitive to tectonic or climatic conditions. I evaluate this hypothesis by investigating the geometry of hillslopes in the tectonically and climatically diverse regions of the Oregon Coast Range (OCR), Gabilan Mesa (GM), and Appalachian Mountains of North Carolina (NC).

Hillslopes that display non-parabolic contour-normal profiles add validity to the steady state form suggested by (4.7) and provide an opportunity to obtain information about key parameters in (2.3). From topographic data, we are able to extract information from profiles that provides estimates of the ratio of uplift rate, W, to activity of transport processes, $E_1\lambda_0$, a quantity referred to as R'. Furthermore, we use previously published estimates of uplift rate in these locations to obtain estimates of $E_1\lambda_0$. By investigating these values in the tectonically and climatically diverse regions of OCR, GM, and NC, we are able to observe the impact that transport processes have on hillslope relief.

Oregon Coast Range

The southern Oregon Coast Range offers an excellent opportunity for morphologic extraction of parameters and exploration of a nonlocal transport formula. The landscape is composed of steep, soil-mantled hillslopes bound by incising mixed alluvial-bedrock channels. Nearly two meters of precipitation falls annually and supports a Douglas Fir forest. Tree throw and dry-

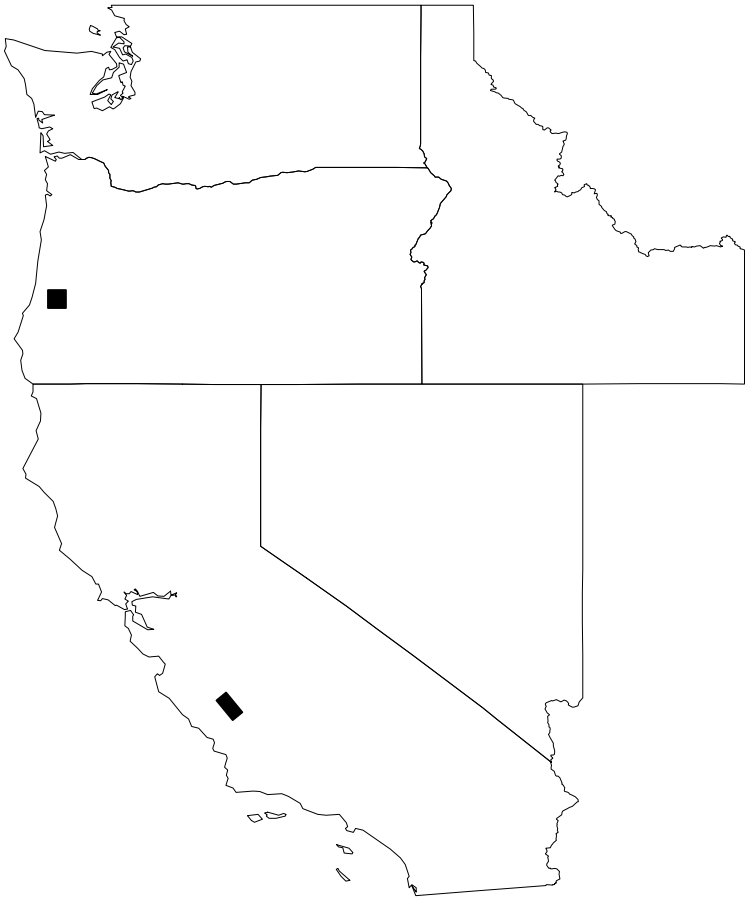

Figure 7: Map showing the location of the Oregon Coast Range and the Gabilan Mesa

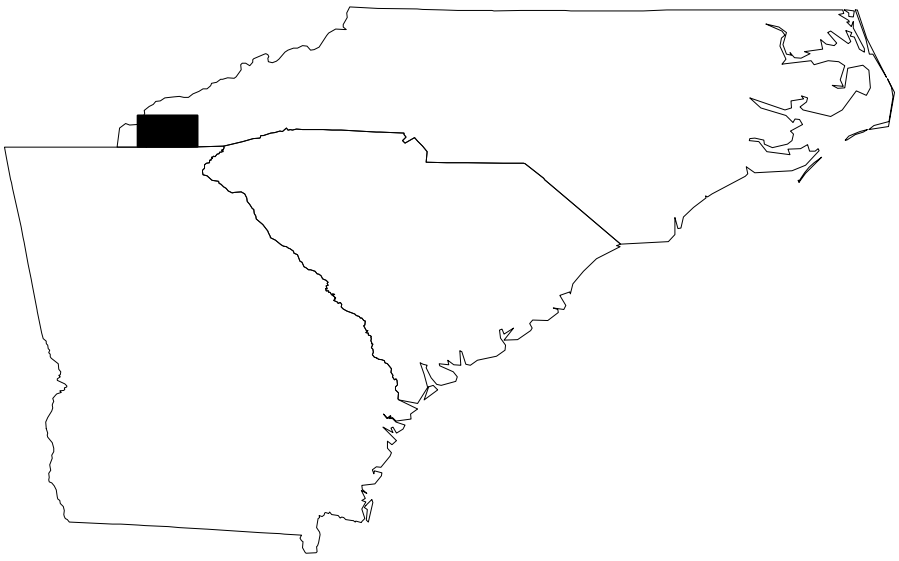

Figure 8: Map showing the location of the site in North Carolina

ravel in post-fire settings are significant sediment transport mechanisms on planar portions of hillslopes ([*Heimsath et al.*, 2001; *Jackson and Roering*, 2009]). Sediment that accumulates in hollows (convergent topography) is frequently evacuated by debris flows and shallow landslides [*Reneau and Dietrich*, 1991]. The region is uniformly underlain by the relatively flat-lying Tyee Formation, a thick sequence of Eocene turbidites [*Snavely et al.*, 1964]. Convergence at the Cascadia subduction zone has driven steady uplift of the region since the Miocene. Spatially uniform estimates of erosion rates [*Reneau and Dietrich*, 1991; *Heimsath et al.*, 2001] are similar to uplift rates [*Kelsey et al.*, 1996], which leads to the broad claim that the region is in an approximate steady state. Average rates for uplift and erosion is about 1×10^{-4} m yr^{-1} for both [*Roering et al.*, 2007].

Gabilan Mesa

The Gabilan Mesa is located in central Salinas Valley of southern California. It is a narrow region of dissected topography bound by the Salinas River to the west and the San Andreas Rift Valley to the east. The Pliocene Pancho Rico and Plio-Pleistocene Paso Robles Formations comprise a weak bedrock substrate [*Roering et al.*, 2007; *Galehouse*, 1967]. Incision of the Salinas River due to uplift on the Rinconada-Reliz fault zone began in the late Pleistocene, and led to widespread dissection of the mesa. The total relief of the mesa is 120 meters which is relatively low compared to OCR. The mediterranean climate provides 32 cm of rainfall annually [*Perron et al.*, 2012] which supports an oak savannah [*Roering et al.*, 2007]. Long term erosion rates estimated by dividing the depth of the major valleys (80 ± 1) by the age of the relict mesa surface ($225 + 239/-139$ kyr) yields a rate of 3.6×10^{-4} m yr^{-1} [*Roering et al.*, 2007]. The GM is characterized by remarkably uniform valley spacing and hilltop concavity, both of which indicate that hillslopes have reached an approximate steady state condition

[*Perron et al.*, 2012].

North Carolina

The Appalachian Mountains of North Carolina comprise a high relief, steep, soil-mantled landscape that supports an oak-hickory forest. Mean annual precipitation is 1.39 m which is distributed evenly throughout the year. Major sediment transport mechanisms appear to be tree throw on planar hillslopes [*Jungers et al.*, 2009] with significant amounts of landsliding that occurs in steep hollows [*Hales et al.*, 2012].

The region is located within the Blue Ridge tectonic province bound by the Valley and Ridge province to the west and the Inner Piedmont to the east. A long and complex geologic history has led to a diverse set of lithologies that include clastic sedimentary, metasedimentary, and metavolcanic rocks interspersed with granitic plutons and ultramafic rocks. Beginning in the Ordivician with the Taconic Orogeny, several east-dipping thrust faults formed in the Blue Ridge Province and were active through the Acadian and Alleghenian Orogenies with deformation ending in the middle Triassic [*Secor et al.*, 1986; *Hatcher and Odom*, 1980].

Since the end of the Alleghenian Orogeny, constant unroofing has resulted in steady uplift driven by the isostatic response of the thick mountain root. Basin average erosion rates estimated by cosmogenic radionuclide analysis reveal an erosion rate of $2.5 \pm 0.5 \times 10^{-5}$ m yr^{-1} within the Great Smoky Mountain National Park, which is consistent with long-term fission track estimates of unroofing from other portions of the Appalachians [*Matmon et al.*, 2003]. Such temporal and spatial consistency between erosion rates has led some researchers to claim that the Appalachian Mountains are in an approximate steady state. Other researchers challenge this claim by pointing to geomorphic evidence in channel-long profiles containing knickpoints that appear to indicate a recent increase in incision [*Gallen et al.*, 2013]. These observations suggest that a four-fold increase in erosion rates from $6.0 \pm 6.0 \times 10^{-6}$ m yr^{-1} to

$2.7 \pm 0.11 \times 10^{-5}$ m yr^{-1}, is migrating up channels as a wave of incision. Maximum knickpoint migration rates in the Cullasaja River Basin are roughly 2×10^{-3} m yr^{-1} and knickpoints are spread over 20 km. This suggests that this portion of the landscape has been slowly adjusting to increased incision rates over 10 myr. A comparison with the hillslope relaxation timescale, which is thought to be about 10^5 years [*Mudd and Furbish*, 2007] reveals that hillslopes may be adjusting to increased incision rates fast enough to keep up with migrating knickpoints. These observations suggest that, although the landscape may be in a long-term transient state, erosion rates change slowly enough for hillslopes to approach an approximate steady-state form. Therefore, the Appalachians are a defensible field site for morphologic tuning of a nonlocal formulation.

Methods

To evaluate the form of hillslopes and obtain estimates of R', the ratio of uplift rate to transport activity, I extract topographic profiles from digital elevation models (DEMs) using ArcGIS software. Because (4.7) is derived from a one-dimensional formulation for the flux, I take care to extract topographic profiles from convex, plan-form planar hillslopes. That is, (4.7) only applies to the portion of hillslopes that do not contain convergent (hollows) or divergent (ridges) topography. For convex-concave hillslopes, I only analyze the convex portions. In an attempt to provide the most robust estimates of quantities I obtained profiles from all aspects. In North Carolina where the lithologies are highly variable, I sampled over various rock-types to obtain a regional estimate of parametric values. The best-fit power relationship is obtained by a performing a linear regression on log transformed data of drop-from-ridge versus position. Most profiles display relationships that are close to a simple power relationship and therefore justify this method (Figure 9).

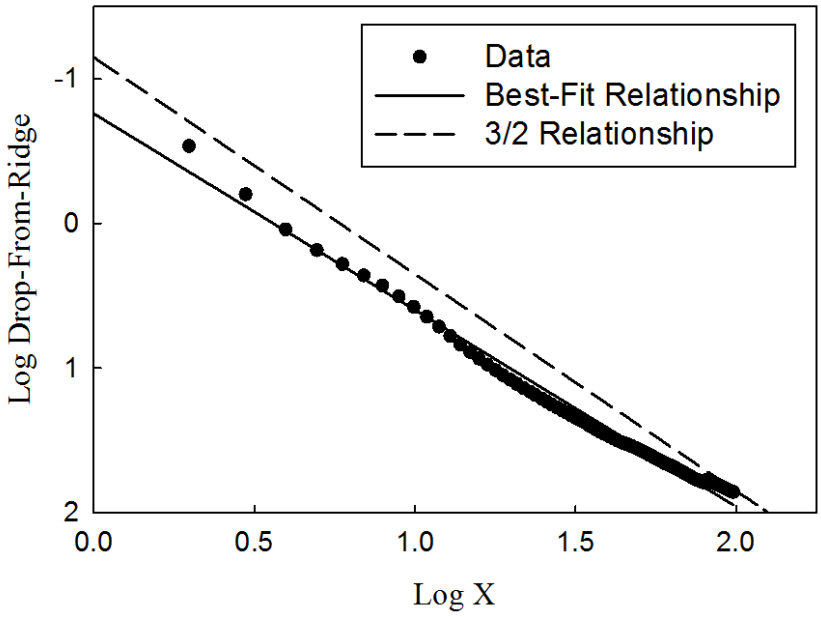

Figure 9: Log Drop-From-Ridge versus log x of a typical hillslope profile. This particular profile is from OCR. The dashed line is the best fit line, with a slope of ≈ 1.4 and the solid line is the theoretical 3/2.

To obtain estimates of R', I rearrange (4.7) such that all measurable quantities are isolated,

$$\left(\frac{2}{S_c} + \frac{1}{kS_p}\right)\left(\frac{3Z_d(x)}{2x^{3/2}}\right)^2 = \frac{c_\eta W}{E_1 \lambda_0}. \tag{5.1}$$

I obtain the measureable quantities from positions where slopes are steep to ensure that I analyzed the portion of the hillslope where nonlocal motions dominate.

One caveat to using such distal positions from the ridge to obtain estimates of R' lies in the sensitivity of a low position to variable incision rates. Because perturbations propagate uphill from the channel and progressively attenuate [*Mudd and Furbish*, 2007], distal positions are more likely to be influenced by variable incision rates. However, I suggest that the ratio of Z_d to x is insensitive to reasonable deviations from the steady-state value for Z_d such that it reflects the dominant conditions.

When W is known, we can solve (5.1) for $E_1\lambda_0$ [$\mathrm{L}^2\mathrm{T}^{-1}$]. Rearranging (5.1) we have,

$$\frac{1}{\left(\frac{2}{S_c}+\frac{1}{kS_p}\right)}\frac{c_\eta W}{\left(\frac{3Z_d}{2x^{3/2}}\right)^2}=E_1\lambda_0. \tag{5.2}$$

Again, all measureable quantities are on the left of (5.2) and yield an estimate of $E_1\lambda_0$.

Chapter 6

RESULTS

Hillslope Form

Data from all sites show similar mean values for the best-fit power relationship between Z_d and position that cluster around 3/2. Such similarity supports the theory suggested by (4.7). There is considerable spread about the mean values; however it is important to note that the majority of these profiles exhibit distinctly non-parabolic forms. Furthermore, the cluster of best-fit power values around 3/2 suggests that these landscapes are likely characterized by Pe greater than ten. Thus, I claim that nonlocal motions dominate the hillslope sediment flux and largely determine the form of the hillslope. This further justifies the use of (4.7) for determining values of R' and $E_1\lambda_0$.

Hillslope Relief

Estimates of R' are consistent with knowledge of uplift rates. The OCR, with an uplift rate of 1.0×10^{-4} m yr^{-1} has the greatest value of $R' = 0.037$ m^{-1} followed by NC with an uplift rate of 2.7×10^{-5} m yr^{-1} and R' of 0.025 m^{-1}. The GM is characterized by the lowest estimate of R' at 0.0003 m^{-1} (Figure 11). However, the semi-arid environment of the GM precludes a simple comparison between the GM, OCR and NC, because the dominant transport mechanisms are likely different.

We can make use of (5.2) to quantitatively evaluate differences among transport processes. Mean annual precipitation serves as a rough proxy for the dominant mechanism of sediment transport as it has a major influence on the ecology of a region. Ecology in turn, determines the types and frequency of disturbances likely to entrain and move sediment particles, and

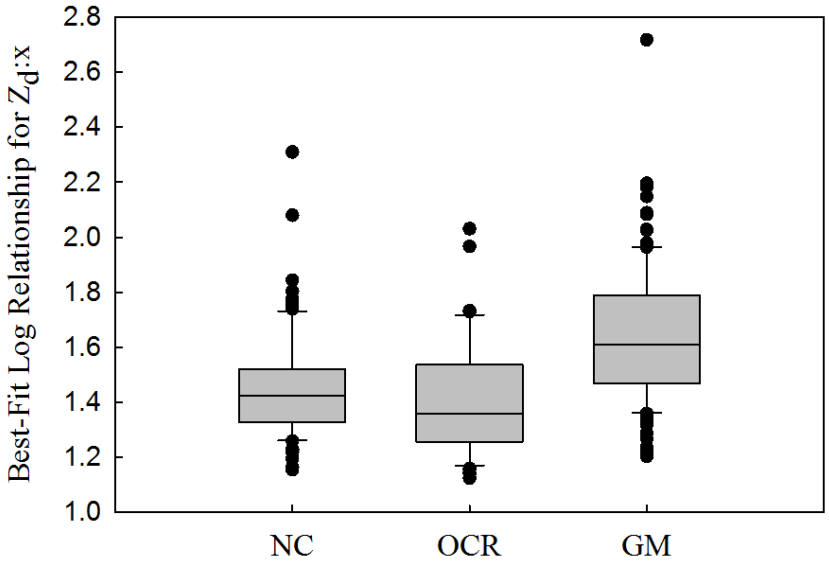

Figure 10: Plot showing the best-fit logarithmic relationship for drop-from ridge and position for NC(n=82), OCR(n=45), and GM(n=117).

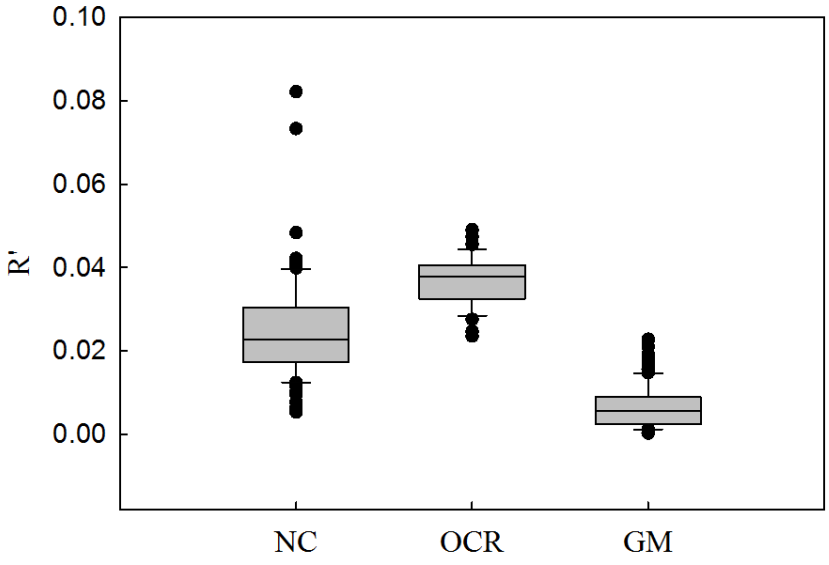

Figure 11: Plot showing the values for R' for NC, OCR, and GM.

therefore is expected to be a first order control on $E_1\lambda_0$. Data from NC and OCR, which receive similar amounts of precipitation and support a similar ecology, reveal similar estimates of $E_1\lambda_0$ of 0.001 and 0.002 m^2 yr^{-1} respectively. This suggests that the transport processes at work in these environments have similar activities. Conversely, topographic data from GM suggest that a different transport mechanism dominates there with a much larger value of estimate for $E_1\lambda_0$ of 0.14 m^2 yr^{-1}. This is consistent with the notion that climate plays a major role in determining the mechanism and activity of transport processes. Less dense vegetation cover that characterizes semi-arid environments does not protect sediment from being entrained which results in more active transport processes.

Chapter 7

DISCUSSION

Data among three sites are consistent with previous findings and expectations. Values of the ratio, R' (5.1), scale with uplift rate for the climatically similar OCR and NC sites (Figure 12), which is consistent with the idea that uplift rate is a primary influence on hillslope relief and average slope. Values of R' from the semi-arid and rapidly uplifting GM are the lowest of the three sites and hints that hillslope relief is also a function of the activity of transport processes. The GM, which is characterized by the lowest relief and mean slope, must evolve by a very active set of transport processes (Figure 12) to balance the rapid uplift rates. Insofar as $E_1\lambda_0$ has units $[\mathrm{L}^2\mathrm{T}^{-1}]$ and represents the activity of transport processes in a region, it can be compared to a diffusivity D from (2.1) and (2.2). Previous researchers observe similar trends in values of diffusivities estimated from hilltop curvature [*Roering et al.*, 2007] for OCR and GM. Although the values of D and $E_1\lambda_0$ cannot be directly compared, the trend for values of $E_1\lambda_0$ between GM and OCR is similar to the trend observed for D, which is consistent with the idea that a more active set of transport processes occur in the GM.

At this point, we are unable to determine specific values of E_1 and λ_0. A high value for $E_1\lambda_0$ may reflect frequent disturbances, long characteristic transport distances, or both. For example, the arid environment of the Gabilan Mesa supports sparse vegetation which may allow for more frequent particle entrainment as sparse vegetation does not provide cohesion or protect sediment from disturbances such as rain drop impacts. Alternatively, an important sediment transport mechanism in the GM is overland flow [*Perron et al.*, 2012] which may have a relatively long characteristic transport distance. In contrast, the major transport process in the OCR and NC is biogenic tree throw, which may have a shorter travel distance and perhaps

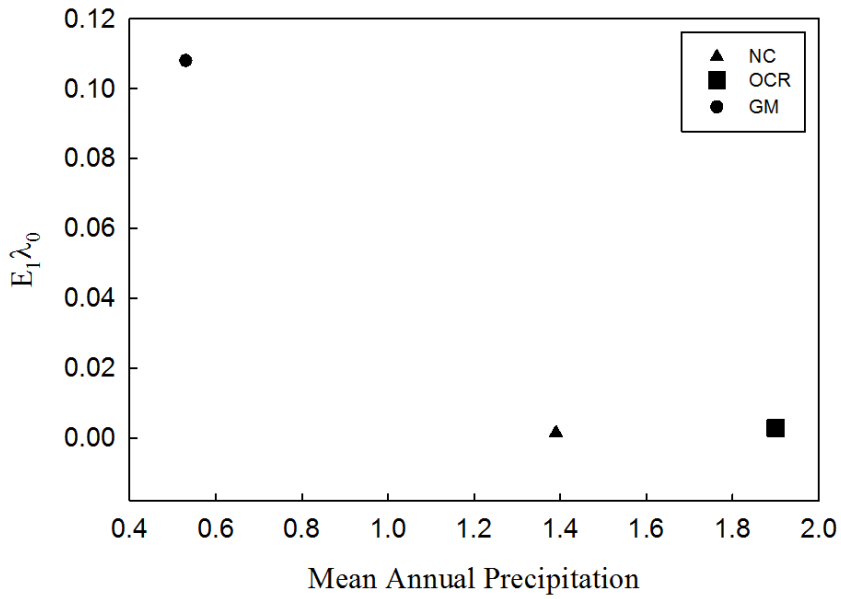

Figure 12: Plot showing values for $E_1\lambda_0$ versus precipitation.

a lower time-averaged entrainment rate, and therefore these landscapes exhibit a lower value of $E_1\lambda_0$. Hillslope relief is consistent with this notion where the mean slope values for NC and OCR are larger than those in the GM.

Using a nonlocal formulation for the hillslope sediment flux offers an opportunity elucidate the relationship between particular transport processes and form. As mentioned above, the form of the disentrainment rate (3.5) is perhaps a simplistic and generalized form. The disentrainment rate may vary depending on the transport mechanism, and the form of (3.5) would be expected to change. Consider a landscape where the majority of the sediment flux comes from nonlocal sediment motions generated by overland flow. A disentrainment rate would likely include the bed shear stress as a primary ingredient as opposed to just the land-surface slope. Indeed formulations for shear stress include S as an ingredient, but writing a disentrainment rate this way weights slope differently. Ultimately, this would have consequences on the overall hillslope form and may deviate from the theoretical $x^{3/2}$ and x^2 relationships

suggested by previous transport formulations. This highlights an opportunity to connect a particular dominant transport process with a specific hillslope geometry as each process may have a unique disentrainment rate.

In any landscape, there is likely to be more than one transport mechanism redistributing sediment. Although one may dominate, the weaker transport processes will still contribute some sediment to the flux, and each process will behave uniquely. Each process will have a characteristic disentrainment rate, and consequently, a unique pdf of particle travel distance. The diverse forms of pdfs will be superimposed on each other leading to a more complex image of particle travel distances. Conceptually,

$$q_x = \int E^1 e^{\int P_r^1} + \int E^2 e^{\int P_r^2} + ... + \int E^n e^{\int P_r^n}, \tag{7.1}$$

where the superscripts refer to the mode of transport. There are many combinations of transport mechanisms and their relative activities, which may lead to unique hillslope forms and relief.

A major challenge for nonlocal transport formulations is determining definitive values for E and λ_0. We must independently obtain values of these parameters in order to draw explicit connections between transport mechanism and hillslope form. This may lie in experimental designs like those used in Gabet and Mendoza [2012] and Abbot [2014], that observe particle travel distance for a single process. The number of particle motions that must be observed for a pdf to converge to a steady form makes this particularly challenging and will require clever experimental designs. Nonetheless, future modelling of more particular transport mechanisms will still be useful [*Gabet et al.*, 2003] and may be able to explain major differences between landscapes.

In particular a feasible next step may be to integrate creep-like motions within the soil

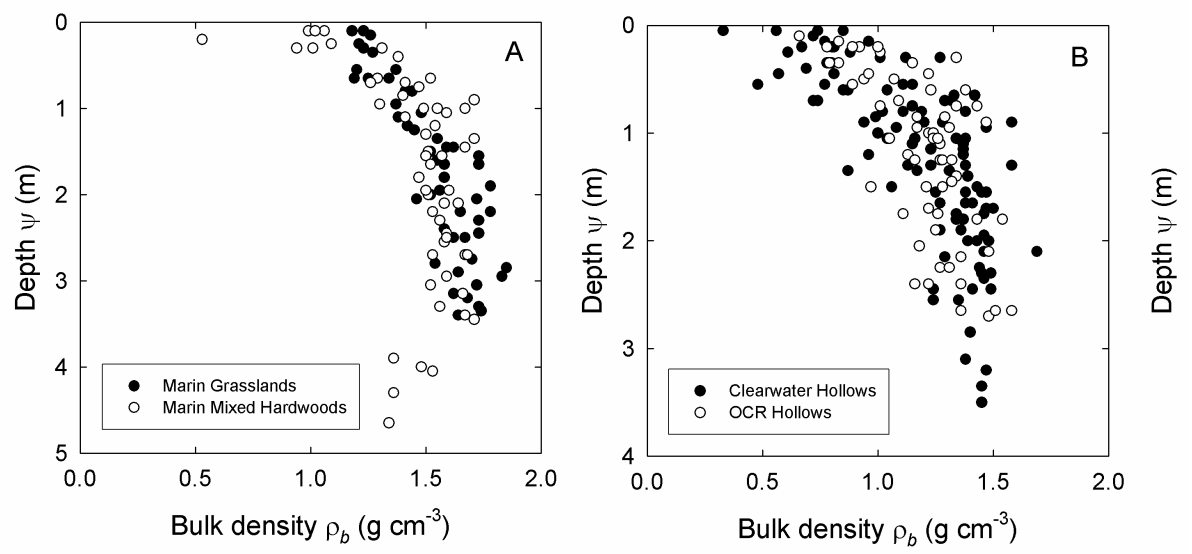

Figure 13: Plots of soil bulk density versus depth into the soil ψ, for soils in (A) Marin County, CA [*Reneau and Dietrich*, 1991] and (B) Clearwater area Washington [*Reneau et al.*, 1989; *Reneau and Dietrich*, 1991].

column with the skittering motions that occur on the surface. The black box of a hillslope diffusivity can be more clearly defined by taking a similar probabilistic approach to what I have presented here. Plots of bulk soil density indicate that soils are vertically stratified and contain more available pore space at shallow depths (Figure 13). More available pore space implies more room for particles to move about. Therefore, we may anticipate that particle travel distances go inversely with depth, ψ, and scale with the mean free path at a particular position within the soil column (Figure 14). We can use this information to develop a formulation for the motions that occur in the soil column that is similar to (3.9). An integration over the entire soil column would include all motions within the column that contribute to the flux. In this way, we are avoiding the somewhat unclear notion of a hillslope diffusivity and are making use of a probabilistic approach that explicitly treats particle travel distance [*Furbish et al.*, 2009a].

Additionally, another pertinent task is to develop a two-dimensional nonlocal formulation

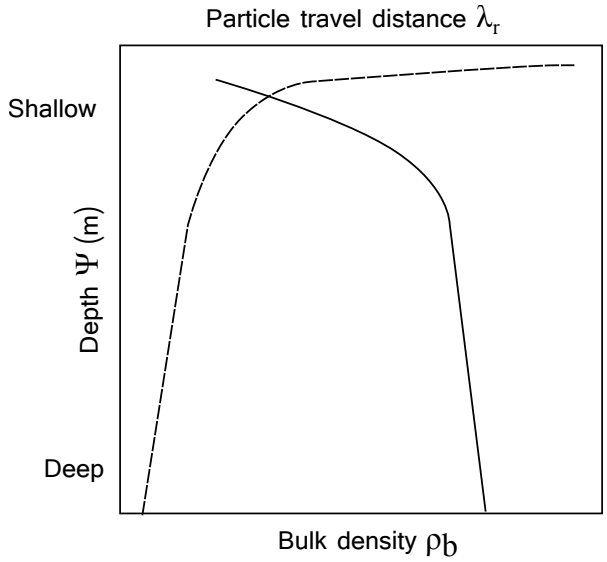

Figure 14: Conceptual plot of soil bulk density ρ_b (solid line) and mean particle travel distance λ_u (dashed line) as functions of soil depth, ψ. Lower bulk density at shallow depths implies increased particle travel distance.

for the hillslope sediment flux. Whereas (3.9) is effective at highlighting the basic hillslope form, it only applies to planar topography. In reality, hillslopes are rarely planar and often contain ridges or hollows, though these may be subtle. A two-dimensional formulation for the hillslope sediment flux will be applicable to any hillslope and will therefore add a greater opportunity to extract information regarding uplift rates and transport processes from landscapes. Furthermore, a two-dimensional formulation may offer insight into the plan view geometry of landscapes that a one-dimensional formulation cannot address. Indeed writing a two-dimensional convolution integral is far more challenging and will be computationally expensive to model through time. However, it is an essential next step in pursuing a deeper understanding of nonlocal transport and its impact on land-surface morphology.

Conclusions

Topographic data from tectonically and climatically diverse landscapes are consistent with modelled hillslope profiles produced by nonlocal sediment transport formulations. The dis-

tinctly non-parabolic forms of steepland landscapes reflects a strong component of nonlocal motions contributing to the flux. The particular form of a hillslope is a result of the relative magnitude of diffusive-like motions to nonlocal, advective-like motions.

Theory suggests that hillslope relief is a function of the competition between uplift rate, w, and the activity of transport processes, $E_1\lambda_0$, which is denoted R' above. We can use topographic data to determine the values of R'. For climatically similar regions, we observe that R' scales with uplift rate, which is consistent with theory. I find that values of R' from climatically different regions do not scale with uplift rate as their dominant transport mechanisms differ and therefore so do their transport activities. Indeed transport activity shows a consistent relationship with mean annual precipitation. This provides a direct link between hillslope relief and transport mechanism, which is strongly affected by climate.

Part II

Hillslope Stability

Chapter 8

INTRODUCTION

In this chapter, I investigate the stability behavior of hillslopes evolving by nonlocal sediment transport. A stability analysis elucidates the response of a system to perturbations about a steady state condition, which may be of two forms. A stable system will respond by attenuating perturbations such that the system returns to its initial steady state condition. In contrast, unstable systems will amplify perturbations at characteristic wavelengths. Previous research shows that linear slope-dependent transport processes are unconditionally stable [*Furbish and Fagherazzi*, 2001]. However, nonlocal sediment particle motions may introduce an instability to hillslopes such that perturbations persist and grow with time. If nonlocal sediment transport introduces an instability to the land-surface behavior, then we expect hillslopes to display topographic roughness with a characteristic scale that reflects the preferred wavelength of growth of disturbances.

Roughness may also be expressed in the spatial distribution of soil thickness, the distance between the land-surface and the soil-saprolite interface, which has implications for the interpretation of the soil-mantle thickness and spatial patterns of land-surface lowering. Research shows that soil thickness has a primary influence on the rate of soil production [*Heimsath et al.*, 2001; *Wilkinson et al.*, 2005], and therefore the local rate of bedrock lowering. In landscapes where the soil thickness is spatially uniform, then bedrock at all points in the landscape lowers at the same rate, which is one definition of morphologic steady state. Researchers often use the spatial distribution of soil thickness as a rough proxy for the state of landscapes (i.e., steady versus transient). Unstable hillslope behavior introduced by the sediment transport mechanism would produce local deviations from a mean soil thickness that would appear to

indicate a transient state. However, because roughness due to an instability may migrate with some celerity, the time-averaged soil thickness may approach a constant mean value. The time-averaged rate of soil production, then, can be uniform while the extant configuration is variable. In order to improve our understanding of the spatial distribution of soil thickness, we must first determine the stability behavior of hillslopes.

In this chapter, I conduct stability analyses of two different formulations for nonlocal transport. The first is a formulation presented in Furbish and Haff [2010] with uniform entrainment rate E. For this formulation I am able to use a linear stability analysis. Secondly, I conduct a numerical stability analysis that elucidates the stability hillslopes evolving by a nonlocal formulation that includes a slope-dependent entrainment rate and a Taylor expansion of the land-surface configuration.

Chapter 9

LINEAR STABILITY ANALYSIS

A linear stability analysis is a convenient analytical method for determining the stability behavior of a system. The analysis applies infinitesimal fluctuations about a defined basic state condition. The evolution of fluctuations is expressed in their time-derivative, which determines if they grow or decay with time. A positive growth rate defines an unstable system, whereas a negative growth rate defines a stable system.

We can couple the evolution of two variables to investigate their co-evolution. In the case of soil-mantled hillslopes, we are interested in the thickening or thinning of the soil mantle. To accomplish this, I couple the co-evolution of fluctuations about the basic state condition for the land-surface, $\zeta(x,t)$, and the soil-saprolite interface, $\eta(x,t)$. I use this method to investigate the stability behavior of hillslopes that evolve under a nonlocal formulation for the sediment flux with a uniform entrainment rate [*Furbish and Haff*, 2010], which is

$$q_x(x,t) = -ES(x',t)\left(\frac{2S_c}{S_c - S(x',t)} - 1\right). \tag{9.1}$$

This must be recast into advection-diffusion form,

$$q_x(x,t) = E\mu_\lambda - E\frac{\mathrm{d}}{\mathrm{d}x}\sigma_\lambda^2, \tag{9.2}$$

where μ_λ and σ_λ^2 are the mean and raw variance of particle travel distances respectively.

Furthermore,

$$\mu_\lambda = -\lambda S(x',t)\left(\frac{2}{S_c}+\frac{1}{S_p}\right) \tag{9.3}$$

$$\begin{aligned}\sigma_\lambda^2 &= \mu_s^2 p + \mu_r^2 n \\ &= \lambda_0^2\left[1+S(x',t)^2\left(\frac{5}{S_c^2}+\frac{4}{S_c S_p}\right)\right],\end{aligned} \tag{9.4}$$

where p and n are the probability of motion in the positive, s, and negative, r, directions respectively. Substituting (9.3) and (9.4) into (9.1) gives

$$q(x,t) = -E\lambda_0\left(\frac{2}{S_c}+\frac{1}{S_p}\right)\left(\frac{\mathrm{d}\zeta}{\mathrm{d}x}\right) - 2E\lambda_0\left(\frac{\mathrm{d}\zeta}{\mathrm{d}x}\right)\left(\frac{\mathrm{d}^2\zeta}{\mathrm{d}x^2}\right)\left(\frac{5}{S_c^2}+\frac{4}{S_c S_p}\right). \tag{9.5}$$

Note that the diffusive term is a nonlinear term that involves the product of the land-surface slope with concavity. Taking only the linear terms, as they will dominate the flux for infinitesimal perturbations, we can simplify to

$$q(x,t) = -E\lambda_0\left(\frac{2}{Sc}+\frac{1}{Sp}\right)\left(\frac{\mathrm{d}\zeta}{\mathrm{d}x}\right). \tag{9.6}$$

The steady state hillslope configuration for hillslopes evolving by (9.6) is

$$\zeta(x) = Z_0 - \frac{WC_\eta x^2}{2E\lambda_0\left(\frac{2}{S_c}+\frac{1}{S_p}\right)}, \tag{9.7}$$

where Z_0 is the ridge-top elevation and C_η is the volumetric particle concentration at the soil saprolite interface. Equation (9.7) defines the basic state condition for the land-surface configuration.

To couple the land-surface with soil thickness I also need to define a basic state condition

for soil production. There is a large body of research that pursues a functional description of the rate of soil production [*Heimsath et al.*, 1997; *Wilkinson et al.*, 2005]. Most functional descriptions of soil production are based on the idea that chemical and physical gradients drive the reactions and processes that weaken bedrock and transform it into soil. Chemical disequilibrium between the Earth's atmosphere and freshly exposed bedrock drives chemical reactions that tend to weaken rock. Hydrologic and temperature gradients further weaken weathered rock and augment the process. Physical disturbances from biologic churning within soil columns also tend to aid in breaking parent material down into soil.

For this investigation I use a 'humped' soil production function. This is a class of functions that place the maximum rate of soil production at some intermediate depth. The reasoning behind this type of function arises from the notion that an intermediate soil depth can sustain chemical and physical processes that weather bedrock while maintaining steep chemical and physical gradients. One such description is

$$P_0 = \alpha \left(\frac{T(x)}{T_\alpha} \right) e^{\left(1 - \frac{T(x)}{T_\alpha}\right)}, \tag{9.8}$$

where P_0 is the production rate [L T^{-1}], $T(x) = \zeta(x) - \eta(x)$ is the soil thickness, T_α is the thickness at which soil production is greatest, and α is the maximum soil production rate. At steady state, the rate of soil production balances the uplift rate and defines the basic state condition used in the stability analysis.

The stability analysis requires a statement of conservation of mass that describes the evolution of the land-surface,

$$\frac{\mathrm{d}\zeta}{\mathrm{d}t} = -\frac{1}{C_\psi}\frac{\mathrm{d}q}{\mathrm{d}x} + \left(1 - \frac{C_\eta}{C_\psi}\right)\left(\frac{\mathrm{d}\eta}{\mathrm{d}t}\right) + C_\eta W, \tag{9.9}$$

where C_ψ is the depth averaged volumetric soil concentration, C_η is the volumetric concentration of the saprolite. The land-surface and soil-saprolite interface are composed of the basic state plus fluctuations about it,

$$\zeta(x,t) = \zeta_0(x,t) + \zeta_1(x,t), \tag{9.10}$$

$$\eta(x,t) = \eta_0(x,t) + \eta_1(x,t), \tag{9.11}$$

where ζ_1 and η_1 are fluctuating quantities about the basic-state variables ζ_0 and η_0 for the land surface and soil saprolite interface respectively. Using (9.8) and (9.9), and placing the fluctuating quantities in appropriate locations gives two expressions that describe the evolution of perturbations,

$$\frac{\mathrm{d}\zeta_1}{\mathrm{d}t} + E\lambda_0 \left(\frac{2}{S_c} + \frac{1}{S_p}\right) \frac{\mathrm{d}^2\zeta_1}{\mathrm{d}x^2} - \left(1 - \frac{C_\eta}{C_\psi}\right) \frac{\mathrm{d}\eta_1}{\mathrm{d}t} = 0 \tag{9.12}$$

$$-P_\alpha e^{\left(1-\frac{\zeta_0-\eta_0}{T_\alpha}\right)} \left(\frac{\zeta_0 - \eta_0}{T_\alpha} - 1\right) (\zeta_1 - \eta_1) - \frac{\mathrm{d}\eta_1}{\mathrm{d}t} = 0 \tag{9.13}$$

The fluctuating quantities are described by ,

$$\zeta_1 = A_\zeta e^{i(m\chi x)+\sigma t}, \tag{9.14}$$

$$\eta_1 = A_\eta e^{(m\chi x)+\sigma t}, \tag{9.15}$$

where A is the amplitude of the perturbation, σ is the growth rate, m is the wavenumber, and $\chi = \pi/X$ where X is the total hillslope length. The product of $m\chi$ ensures that perturbations have wavelengths that are integer factors of the hillslope length, and that the slope at the crest is zero and the slope at the base of the hillslope equals that of the basic state condition. Inserting the definitions of fluctuating quantities into (9.12) and (9.13), and noting that every

term has $e^{i(m\chi x)+\sigma t}$ in it, we obtain

$$\sigma\zeta_1 + \frac{E\lambda_0 m^2\chi^2}{C_\psi}\zeta_1 - \left(1 - \frac{C_\eta}{C_\psi}\right)\sigma\eta_1 = 0, \tag{9.16}$$

and

$$\frac{P_\alpha}{T_\alpha}e^{\left(1-\frac{\zeta_0-\eta_0}{T_\alpha}\right)}\left(\frac{\zeta_0-\eta_0}{T_\alpha}-1\right)\zeta_1 - \frac{P_\alpha}{T_\alpha}e^{\left(1-\frac{\zeta_0-\eta_0}{T_\alpha}\right)}\left(\frac{\zeta_0-\eta_0}{T_\alpha}-1\right)\eta_1 - \sigma = 0. \tag{9.17}$$

The determinant of the system of equations involving (9.16) and (9.17) gives an expression that reveals the growth rate of perturbations when it is solved for σ,

$$\begin{aligned} -\sigma^2 - \sigma\left(\frac{E\lambda_0 m^2\chi^2}{C_\psi} - \frac{C_\eta}{C_\psi}\left[\frac{P_\alpha}{T_\alpha}e^{\left(1-\frac{\zeta_0-\eta_0}{T_\alpha}\right)}\left(\frac{\zeta_0-\eta_0}{T_\alpha}-1\right)\right]\right) + \\ \frac{E\lambda_0 m^2\chi^2}{C_\psi}\left(\frac{P_\alpha}{T_\alpha}e^{\left(1-\frac{\zeta_0-\eta_0}{T_\alpha}\right)}\left[\frac{\zeta_0-\eta_0}{T_\alpha}-1\right]\right) = 0. \end{aligned} \tag{9.18}$$

If the solution for σ is negative, the system is stable as the amplitude of perturbations decreases with time. A positive solution for σ reveals an unstable system as the perturbations grow with time. There are two scenarios I test, and each scenario has two solutions. One solution refers to the stability of the soil thicknes and the other to the land-surface. The first scenario places the basic state soil thickness $(\zeta_0 - \eta_0)$ on the left side of T_α, where soil is thinner than the depth at which maximum soil production occurs, T_α. In this case, we see that all wave numbers are unstable reflecting the instability inherent in a humped soil production function. Growth rates are highest for perturbations with low wave numbers, indicating that larger perturbations will grow faster (Figure 15) and will dominate the roughness scale of soil thickness.

An alternative scenario places the basic state soil thickness greater than T_α. In this case,

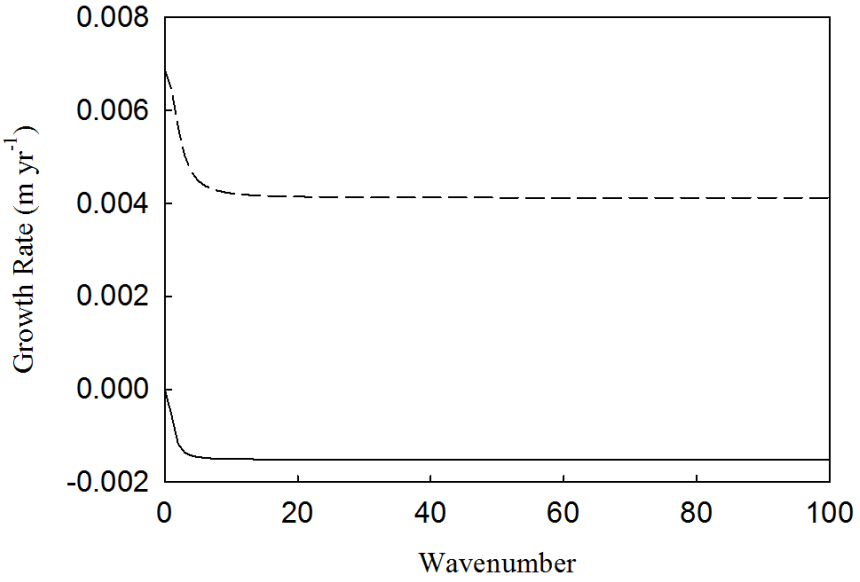

Figure 15: A stability plot for soil thickness. The dashed line is the condition for which the initial state has a soil thickness less than T_α. The solid line has an initial condition with the soil thickness greater than T_α.

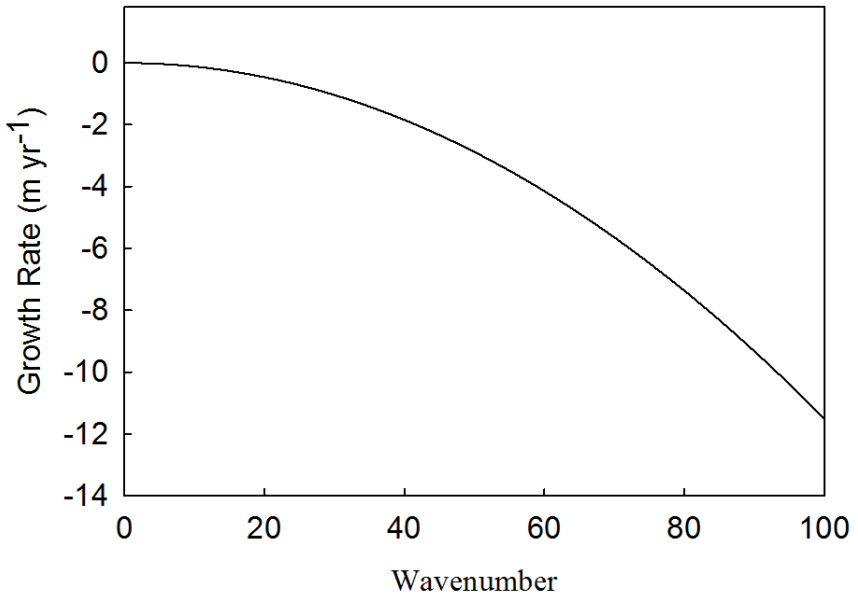

Figure 16: A stability field for the land-surface only. All wavenumbers decay with the smaller perturbations decaying the most rapidly.

perturbations of all wavenumbers are stable, with increasingly negative growth rates correlating with larger wavenumbers. This indicates that smaller perturbations are more rapidly smoothed (Figure 15).

The behavior of the land-surface is determined by the other solution for (9.18). For both scenarios, the land-surface has the same stability behavior. Results for this analysis show that the land-surface is stable for all wavenumbers (Figure 16). Such stable behavior of the land-surface is the same conclusion that Furbish and Fagherazzi [2001] came to for linear hillslope diffusion. This suggests that, with a uniform entrainment rate, nonlocal and local diffusive transport behave similarly.

Chapter 10

NUMERICAL STABILITY ANALYSIS

In this section I present a numerical stability analysis that determines the stability behavior of hillslopes evolving by nonlocal transport with a non-uniform entrainment rate. A numerical stability analysis consists of perturbing the steady state condition with a disturbance of finite amplitude and varying wavelengths. The stability behavior is observed by watching the perturbations evolve over several time steps (3 to 5). The growth rate is determined by taking the difference in elevation at successive time steps. Here, the magnitude of the growth rate is not significant in itself, but the sign of it is, where negative growth rates indicate stable behavior and positive growth rates indicate unstable behavior.

I develop this formulation from a disentrainment rate that includes the first term of a Taylor series expansion of slope. This addition gives the formulation an ability to 'look' downhill and adjust to changing conditions. Therefore the disentrainment rate is not simply a function of the slope at x', but approximates the terrain immediately downslope, which particles will travel over. The disentrainment rate goes as,

$$P_r = \frac{1}{\lambda_0}\left(\frac{2S_c}{S_c - S_{x'} - \frac{\mathrm{d}S_{x'}}{\mathrm{d}x}r} - 1\right) \tag{10.1}$$

where r is the distance upslope from x to x'. The formulation developed from this disentrainment rate is,

$$q_p = \int_{-\infty}^{0} P_{x',t}\left(E_0 + E_1|S_{x',t}|\right) e^{\frac{r}{\lambda_0}} \left(\frac{S_c - S_{x',t} - \frac{\mathrm{d}S_{x',t}}{\mathrm{d}x}r}{S_c - S_{x',t}}\right)^{\left(\frac{2S_c}{\lambda_0 \frac{\mathrm{d}S}{\mathrm{d}x}}\right)} \mathrm{d}x', \tag{10.2}$$

where q_p is the flux in the positive x direction, and P is the probability of motion in the

positive direction. The flux in the negative direction goes as

$$q_n = -\int_{-\infty}^{0} N_{x',t}\left(E_0 + E_1|S_{x',t}|\right) e^{\frac{r}{\lambda_0}} \left(\frac{S_c + S_{x',t} - \frac{\mathrm{d}S_{x',t}}{\mathrm{d}x} r}{S_c + S_{x',t}}\right)^{\left(\frac{2S_c}{\lambda_0 \frac{\mathrm{d}S}{\mathrm{d}x}}\right)} \mathrm{d}x', \qquad (10.3)$$

where N is the probability of motion in the negative x direction. The total flux is the sum of (10.2) and (10.3). These forms are not analytically integrable, which requires that we perform a numerical integration to determine the flux. This limitation precludes the use of a linear stability analysis and requires a numerical analysis to determine the stability behavior of this formulation.

The results show that hillslopes are unstable for particular combinations of E_1 and λ_0. In general, greater values of $E_1\lambda_0$ lead to higher instability. The growth rates are sensitive to the land-surface slope at a given position; generally, greater growth rates occur on steeper slopes. This finding indicates that as nonlocal transport becomes stronger, it introduces more instability. Alternatively stated, greater advection leads to instability and higher growth rates. For the particular set of parameters chosen, the analysis reveals that topographic roughness with scales of 1-4 meters may be expected (Figure 17). To test this hypothesis, I examine the topographic roughness on real hillslopes.

To determine the roughness scales on hillslopes, I apply a wavelet analysis to a high resolution (1 m) topographic data set. Wavelets are analogous to a classic spectral analysis in that they determine the fit of a periodic function to the observed data; however, there are some important differences. A spectral analysis assumes that frequencies in a series are consistent. That is, any frequency in a series is expected to be present throughout the signal at the same strength. A wavelet analysis does not make this assumption and therefore affords slightly more freedom in that the analysis returns both frequency and position information. This is useful for exploring hillslope roughness because the roughness scale may change with slope,

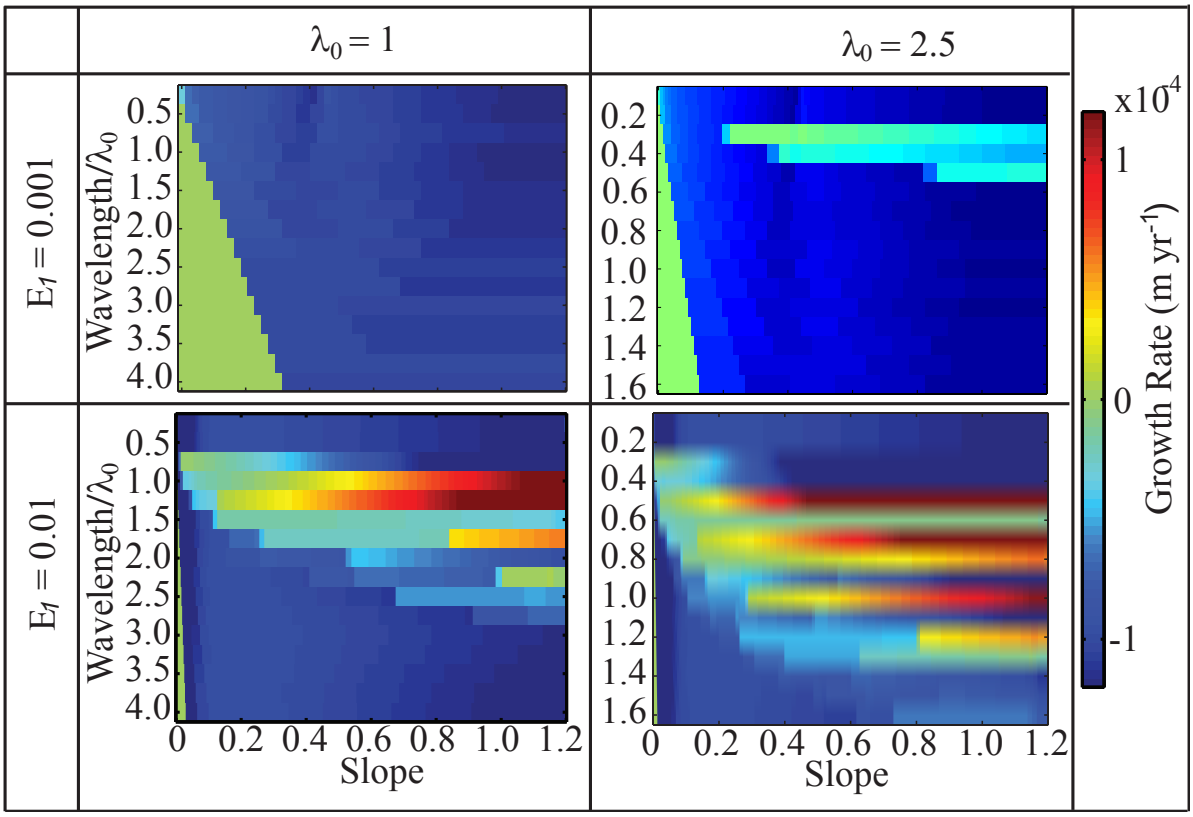

Figure 17: A plot of stability fields for various combinations of parameters. Warm colors indicate positive growth rates and therefore unstable wavelengths for particular slopes. Cool colors indicate negative growth rates. Hillslopes appear to be most unstable for wavelengths similar to λ_0.

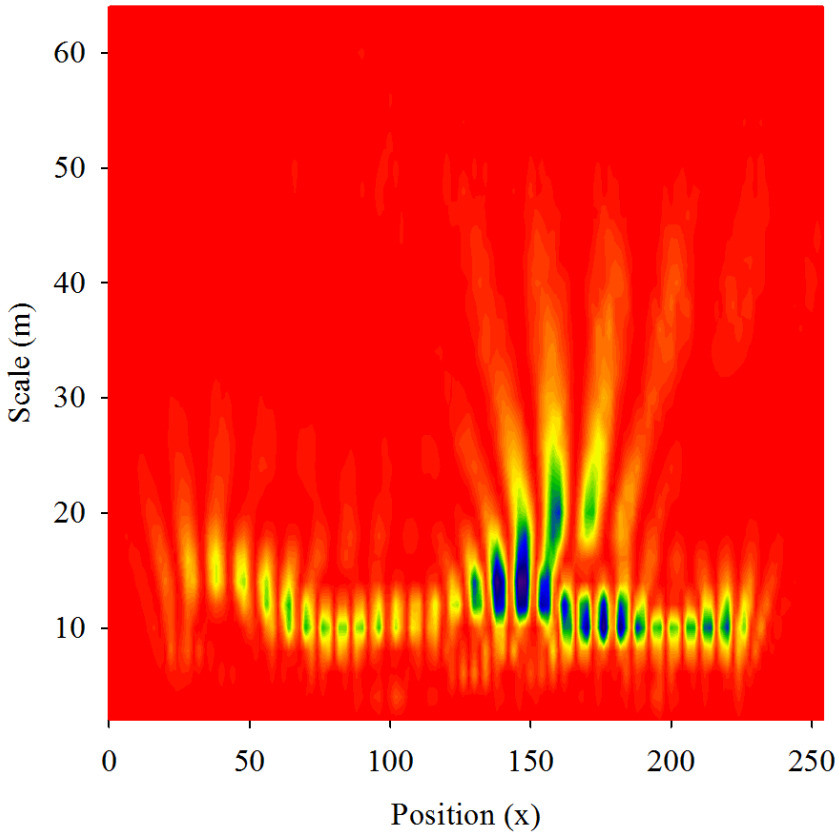

Figure 18: Wavelet power spectrum of detrended land-surface elevation. Warm colors indicate low power and cool colors indicate high power.

and therefore with location along the hillslope.

I will present only one wavelet analysis here, although I performed others that produced similar results. The hillslope analyzed is located in southwestern North Carolina, just north of the Coweeta Long Term Ecological Research Station. It is a steep, soil-mantled hillslope with a northerly aspect and maximum slopes that reach ≈ 0.5. The hillslope is densely populated with oak, hickory, and rhododendron trees. I first detrended the topographic data using a Loess filter with a window equal to twenty percent of the entire signal length, which was 230 meters long. A wavelet analysis reveals a persistent roughness scale in the land-surface elevation that has a 12 meter wavelength (Figure 18). This wavelength appears to occur

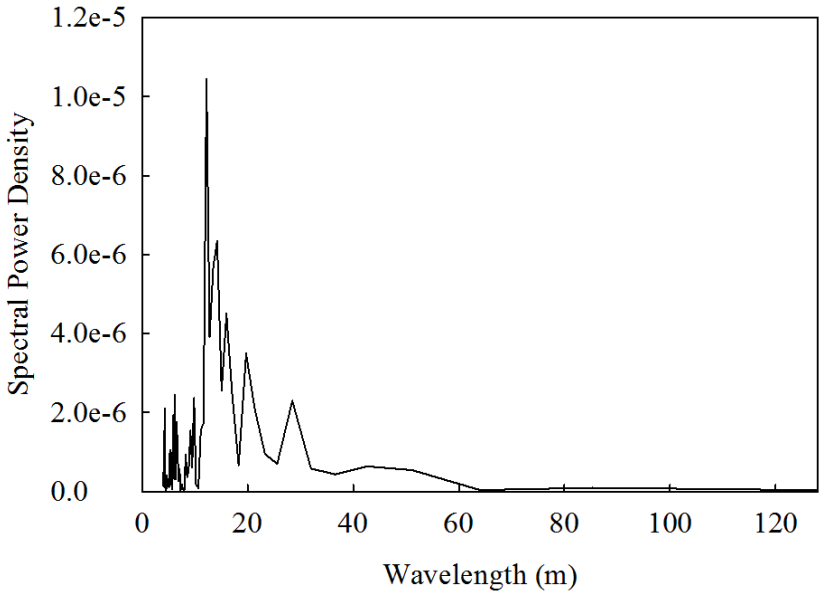

Figure 19: Spectral density plot of detrended surface elevation.

somewhat periodically which justifies the use of a classic spectral analysis. This also identifies a roughness scale with a 12 meter period as the dominant signal (Figure 19). This scale is slightly longer but not inconsistent with that predicted by the numerical analysis.

This same roughness scale is also observed in soil thickness data taken from the same profile. Following the same methods as outlined above for the land-surface elevation, I conducted wavelet and spectral analyses on the soil thickness data. The wavelet output identifies a consistent roughness scale that varies from 10 to 20 meters (Figure 20). These scales are also persistent throughout the hillslope, and justify using a classic spectral analysis , which reveals two dominant peaks; one at 12 meters and another at 18 meters (Figure 21). There is a strong similarity between the roughness scales of soil depth and topography which suggests that the geometry of the soil-saprolite surface is similar to the land-surface.

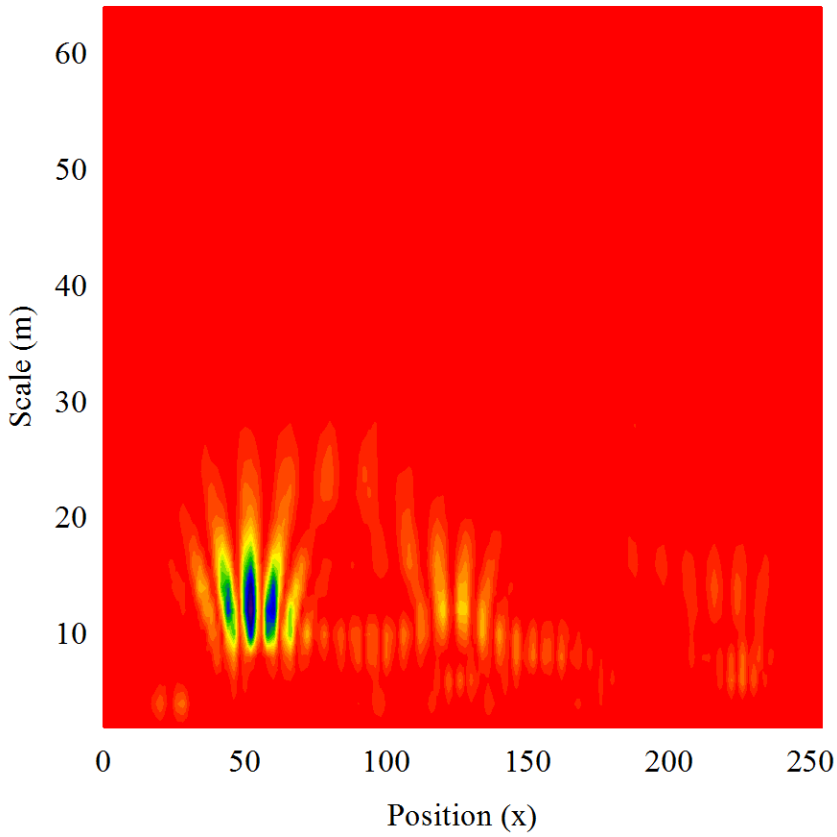

Figure 20: Wavelet power spectrum of soil thickness, where cool colors indicate high power and warm colors indicate low power.

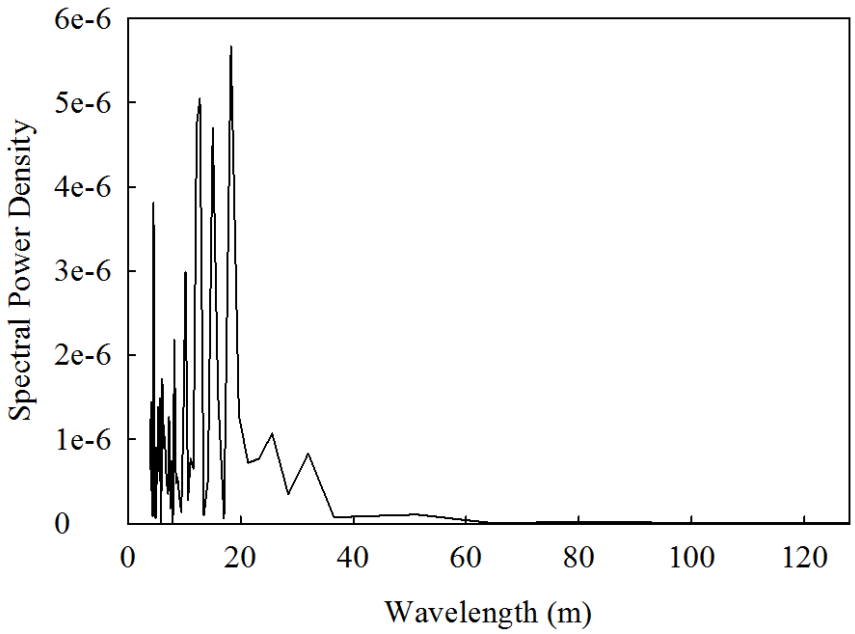

Figure 21: Spectral density plot of detrended soil thickness data.

Chapter 11

DISCUSSION

The linear stability analysis of hillslopes that evolve by a sediment transport formulation with a uniform entrainment rate reveals that such descriptions are unconditionally stable. This result then suggests that the roughness that exists on hillslopes is primarily caused by the main disturbing agents (i.e. tree throw, gopher mounds), and the roughness scales will reflect this [*Jyotsna and Haff*, 1997]. If this is indeed true, then roughness scales would be expected to be the same in both down-slope and cross-slope directions. Further field work will need to be done in order to provide this data.

Although topographic roughness observed in the field is similar to scales expected from the numerical stability analysis, it will be difficult to definitively assign causality to the origin of topographic roughness. In previously published literature, roughness scales are interpreted as a product of the primary disturbing mechanisms [*Jyotsna and Haff*, 1997; *Roering et al.*, 2010]. Roering et al., [2010] analyzed several 25 meter sections of a hillslope using ground-penetrating radar to obtain trends in soil depth. They identified a dominant 5 meter roughness scale, which they attributed to the signature of the biological disturbances caused by Douglas Fir trees in the Oregon Coast Range. Although in the same study, there appears to be a strong 10 meter signal, which they do not address. The scale identified in North Carolina is longer than 5 meters, which suggests different possible explanations.

The periodic and uniform scale of disturbances in both the land-surface and the soil thickness is consistent with unstable hillslope behavior. Yet, there is a possibility that the roughness we observe reflects the integrated spatial history of growth and decay of trees in a steady state forest. Upended root wads and decaying root mounds may take considerable time to vanish,

during which time new trees will sprout and grow. Therefore roughness in the surface may be a result of the extant trees but also of 'ghost' trees. The highly periodic nature of soil depth and land-surface, however, makes this seem implausible (Figure 18). There is the additionally possibility that surface roughness reflects structural control. This too is unlikely as the strike of the metamorphic foliation is dominantly perpendicular to the trend of the ridge.

Chapter 12

CONCLUSIONS

A linear stability analysis of hillslopes evolving by nonlocal sediment transport reveals that the land-surface is unconditionally stable. This behavior is the same conclusion that Furbish and Fagherazzi [1997] came to for linear, slope-dependent transport. Perturbations are, however, expected to persist in soil thickness for the special case where the initial condition has a basic state soil thickness less than the depth at which maximum soil production occurs, T_α. This simply reflects instability in the humped soil production function and does not reflect anything about the land-surface. That is, the functional form of a humped soil production is inherently unstable for a system with a basic state soil thickness less than T_α.

A numerical stability analysis for a nonlocal formulation that includes a Taylor series expansion of the land-surface slope indicates that the land-surface is unstable for particular combinations of an entrainment rate, E_1, and a characteristic travel distance, λ_0. Indeed a hillslope from North Carolina displays a roughness scale that is not dissimilar from the scale expected from the numerical analysis and is periodic. Other explanations for the periodic topographic roughness observed seem implausible, which lend credibility to an inherent instability as a cause for topographic roughness. Whereas it is not yet possible to definitively say that we can observe instability, the evidence is not inconsistent with numerical stability analyses. Further work is required to identify a difference between the signature of roughness due solely to biology and that due to hillslope instability. Additionally, the similarity between the land-surface and soil-saprolite geometries implies that the two are linked, although causality is difficult to determine.

Culling, W. (1965), Theory of erosion on soil-covered slopes, *The Journal of Geology*, pp. 230–254.

Foufoula-Georgiou, E., V. Ganti, and W. Dietrich (2010), A nonlocal theory of sediment transport on hillslopes, *Journal of Geophysical Research: Earth Surface (2003–2012)*, *115*(F2).

Furbish, D. J., and S. Fagherazzi (2001), Stability of creeping soil and implications for hillslope evolution, *Water Resources Research*, *37*(10), 2607–2618.

Furbish, D. J., and P. K. Haff (2010), From divots to swales: Hillslope sediment transport across divers length scales, *Journal of Geophysical Research: Earth Surface (2003–2012)*, *115*(F3).

Furbish, D. J., and J. J. Roering (2013), Sediment disentrainment and the concept of local versus nonlocal transport on hillslopes, *Journal of Geophysical Research: Earth Surface*.

Furbish, D. J., P. K. Haff, W. E. Dietrich, and A. M. Heimsath (2009a), Statistical description of slope-dependent soil transport and the diffusion-like coefficient, *Journal of Geophysical Research: Earth Surface (2003–2012)*, *114*(F3).

Furbish, D. J., E. M. Childs, P. K. Haff, and M. W. Schmeeckle (2009b), Rain splash of soil grains as a stochastic advection-dispersion process, with implications for desert plant-soil interactions and land-surface evolution, *Journal of Geophysical Research: Earth Surface (2003–2012)*, *114*(F3).

Gabet, E. J., and M. K. Mendoza (2012), Particle transport over rough hillslope surfaces by dry ravel: Experiments and simulations with implications for nonlocal sediment flux, *Journal of Geophysical Research: Earth Surface (2003–2012)*, *117*(F1).

Gabet, E. J., O. Reichman, and E. W. Seabloom (2003), The effects of bioturbation on soil processes and sediment transport, *Annual Review of Earth and Planetary Sciences*, *31*(1), 249–273.

Gabet, E. J., B. A. Pratt-Sitaula, and D. W. Burbank (2004), Climatic controls on hillslope angle and relief in the himalayas, *Geology*, *32*(7), 629–632.

Galehouse, J. S. (1967), Provenance and paleocurrents of the paso robles formation, california, *Geological Society of America Bulletin*, *78*(8), 951–978.

Gallen, S. F., K. W. Wegmann, and D. Bohnenstiehl (2013), Miocene rejuvenation of topographic relief in the southern appalachians, *GSA Today*, *23*(2), 4–10.

Hales, T., K. Scharer, and R. Wooten (2012), Southern appalachian hillslope erosion rates measured by soil and detrital radiocarbon in hollows, *Geomorphology*, *138*(1), 121–129.

Hatcher, R., and A. Odom (1980), Timing of thrusting in the southern appalachians, usa: model for orogeny?, *Journal of the Geological Society*, *137*(3), 321–327.

Heimsath, A. M., W. E. Dietrich, K. Nishiizumi, and R. C. Finkel (1997), The soil production function and landscape equilibrium, *Nature*, *388*(6640), 358–361.

Heimsath, A. M., W. E. Dietrich, K. Nishiizumi, and R. C. Finkel (2001), Stochastic processes of soil production and transport: Erosion rates, topographic variation and cosmogenic nuclides in the oregon coast range, *Earth Surface Processes and Landforms*, *26*(5), 531–552.

Jackson, M., and J. J. Roering (2009), Post-fire geomorphic response in steep, forested landscapes: Oregon coast range, usa, *Quaternary Science Reviews*, *28*(11), 1131–1146.

Jungers, M. C., P. R. Bierman, A. Matmon, K. Nichols, J. Larsen, and R. Finkel (2009), Tracing hillslope sediment production and transport with in situ and meteoric 10be, *Journal of Geophysical Research: Earth Surface (2003–2012)*, *114*(F4).

Jyotsna, R., and P. Haff (1997), Microtopography as an indicator of modern hillslope diffusivity in arid terrain, *Geology*, *25*(8), 695–698.

Kelsey, H. M., R. L. Ticknor, J. G. Bockheim, and E. Mitchell (1996), Quaternary upper plate deformation in coastal oregon, *Geological Society of America Bulletin*, *108*(7), 843–860.

Matmon, A., P. Bierman, J. Larsen, S. Southworth, M. Pavich, and M. Caffee (2003), Temporally and spatially uniform rates of erosion in the southern appalachian great smoky mountains, *Geology*, *31*(2), 155–158.

Mudd, S. M., and D. J. Furbish (2007), Responses of soil-mantled hillslopes to transient channel incision rates, *Journal of Geophysical Research: Earth Surface (2003–2012)*, *112*(F3).

Ouimet, W. B., K. X. Whipple, and D. E. Granger (2009), Beyond threshold hillslopes: Channel adjustment to base-level fall in tectonically active mountain ranges, *Geology*, *37*(7), 579–582.

Perron, J. T., P. W. Richardson, K. L. Ferrier, and M. Lapôtre (2012), The root of branching river networks, *Nature*, *492*(7427), 100–103.

Reneau, S. L., and W. E. Dietrich (1991), Erosion rates in the southern oregon coast range: Evidence for an equilibrium between hillslope erosion and sediment yield, *Earth Surface Processes and Landforms*, *16*(4), 307–322.

Reneau, S. L., W. E. Dietrich, M. Rubin, D. J. Donahue, and A. T. Jull (1989), Analysis of hillslope erosion using dated colluvial deposits, *Journal of Geology;(USA)*, *97*(1).

Roering, J. J., J. W. Kirchner, and W. E. Dietrich (1999), Evidence for nonlinear, diffusive sediment transport on hillslopes and implications for landscape morphology, *Water Resources Research*, *35*(3), 853–870.

Roering, J. J., J. W. Kirchner, and W. E. Dietrich (2001), Hillslope evolution by nonlinear, slope-dependent transport: Steady state morphology and equilibrium adjustment timescales, *Journal of Geophysical Research: Solid Earth (1978–2012)*, *106*(B8), 16,499–16,513.

Roering, J. J., J. T. Perron, and J. W. Kirchner (2007), Functional relationships between denudation and hillslope form and relief, *Earth and Planetary Science Letters*, *264*(1), 245–258.

Roering, J. J., J. Marshall, A. M. Booth, M. Mort, and Q. Jin (2010), Evidence for biotic controls on topography and soil production, *Earth and Planetary Science Letters*, *298*(1), 183–190.

Secor, D. T., A. W. Snoke, and R. D. Dallmeyer (1986), Character of the alleghanian orogeny in the southern appalachians: Part iii. regional tectonic relations, *Geological Society of America Bulletin*, *97*(11), 1345–1353.

Snavely, P. D., H. C. Wagner, and N. S. MacLeod (1964), Rhythmic-bedded eugeosynclinal deposits of the tyee formation, oregon coast range, *Kans. Geol. Surv. Bull*, *169*, 461–480.

Tucker, G. E., and D. N. Bradley (2010), Trouble with diffusion: Reassessing hillslope erosion laws with a particle-based model, *Journal of Geophysical Research*, *115*(null), F00A10.

Whipple, K. X., E. Kirby, and S. H. Brocklehurst (1999), Geomorphic limits to climate-induced increases in topographic relief, *Nature*, *401*(6748), 39–43.

Wilkinson, M. T., J. Chappell, G. S. Humphreys, K. Fifield, B. Smith, and P. Hesse (2005), Soil production in heath and forest, blue mountains, australia: influence of lithology and palaeoclimate, *Earth Surface Processes and Landforms*, *30*(8), 923–934.